Towards Microfluidic Color Detection Using Micropumps

Thesis submitted in partial fulfillment
of the requirements for the degree of

Master of Science in ***Electronics and Communication Engineering*** *by Research*

by

Shreya Malkurthi
2019122001
shreya.malkurthi@research.iiit.ac.in

International Institute of Information Technology
Hyderabad - 500 032, INDIA
June 2023

International Institute of Information Technology

Hyderabad, India

CERTIFICATE

It is certified that the work contained in this thesis, titled **"Towards Microfluidic color detection using Micropumps"** by Shreya Malkurthi, has been carried out under my supervision and is not submitted elsewhere for a degree.

Date

Advisor: Dr. Aftab M. Hussain

To my Family

Acknowledgments

First, I would like to express my heartfelt gratitude to Dr. Aftab Hussain, my thesis supervisor, for his guidance and patience throughout my academic and research journey over the last three years. Not only has he motivated and inspired me, but he has also instilled in me the importance of quality research and teaching. Dr. Hussain's expertise, continuous support, and feedback have been instrumental in refining my ideas and shaping my thesis.

I want to thank Prof. David Clarke for his tremendous support during my time at Harvard University. I am also very thankful to Gino Domel for mentoring me during the project and our productive brainstorming sessions. I want to give a special mention to Ehsan Hajiesmaili for providing valuable insights into a few experiments.

I would like to thank all my labmates from PATRIoT + FleCS lab for contributing to a lively and enjoyable research environment. I especially want to thank Deeksha Devendra for providing guidance and mentorship during the early stages of my research, as well as for being a wonderful friend. I would also like to thank D. Niteesh and Kirthi Vignan for their valuable contributions to the work and for helping me with a few critical experiments. I deeply appreciate their time and effort. I would like to thank my dearest friends (in no particular order), Manaswini Reddy, Nihar Potturu, Rahul Kashyap, Karan Mirakhor, Anushree Korturti, Tushar Patra, Deeksha Devendra, Mohee Datta Gupta, and the whole 'BB GG' group, for their constant love and for making my college life unforgettable.

Lastly, I want to extend my deepest gratitude to my family for their unwavering love and support. Their understanding and belief in me have been a constant source of strength throughout my journey. To all of you who have contributed to my academic journey, thank you for your encouragement, support, and affection. I could not have achieved this without each and every one of you.

Abstract

Microfluidic systems are effective tools for carrying out a wide range of chemical and biological analyses. Utilizing colorimetry in conjunction with microfluidic devices has proven to be a highly effective method for conducting various analyses that require rapid results. Such systems have significant applications in lab-on-a-chip systems and other medical devices that necessitate a colorimetric measurement to obtain quantitative results about the chemical composition of a given sample. Currently, most state-of-the-art techniques for performing microfluidic color detection use expensive cameras to study the captured image or are paper-based analytical devices that use capillary action to analyze color information. However, paper-based microfluidic devices are limited by the evaporation of test samples during experiments and therefore require high volumes of samples. Additionally, the surface tension of the liquid sample plays a crucial role in this process, and if not properly managed, the device may not provide accurate results.

To overcome these limitations, a low-cost automated color detection system that could be used in conjunction with planar microfluidic pumps is presented in this work. The color detection system uses a light-emitting diode (LED) and a light-dependent resistor (LDR) to obtain color information. The LED is used to sequentially shine the primary color component wavelengths - red, green, blue - on the sample, and the color information is obtained from the light intensity incident onto the LDR after reflecting from the sample. The results showed that the system is accurate up to 92% and could be readily readily used to conduct different types of chemical analyses using colorimetry and can be employed in various industries to automate chemical and other biomedical processes completely.

The flexible, planar micropumps discussed in this work are based on a nozzle-diffuser design that employs a central chamber connected to two trapezoidal flow diodes. The pump was fabricated using polydimethylsiloxane (PDMS) as a two-layer structure: a bottom layer with molded channels and the chamber, encapsulated by a planar top layer. The transparency of the pump and biocompatibility of PDMS make it an excellent material for biomedical and colorimetric applications. The pump design was

characterized for its performance, both when placed on a flat surface and surfaces of different bending radii, by counting the number of compression cycles required for a known volume of fluid, here water, to flow from the inlet to the outlet. The pump produced a flow rate per compression cycle of 5.53 μl on a flat surface and that of 4μl, 3.6 μl when placed on surfaces of bending radii of 71cm and 45 cm, respectively. Finally, the pumping mechanism was completely automated by replacing the diaphragm with a dielectric elastomer actuator (DEA) and using a tesla valve for fluidic channels. The pressure difference imparted by the deformation of the actuator when a sinusoidal voltage is applied is converted to fluid flow (velocity). We also propose a microfluidic system that employs three microfluidic pumps and a central color detection module to perform effective microfluidic color detection. The proposed system provides a cost-effective solution for conducting chemical analyses using colorimetric assays.

Contents

List of Figures

Chapter 1

Introduction

Color detection has a wide range of applications ranging from monitoring production processes, product quality, color calibration of displays, paints, textiles, color sorting systems, and so on [91]. In medical sciences, color detection is used with chemical reactions such as water tests, pH tests, titrations, covid tests, and other medical tests [67, 84, 92]. It is an essential aspect of many applications, including image processing, computer vision, robotics, and color printing. It is used in several analytical chemistry processes in various industries such as biomedical, diagnostics, agriculture, food processing, and so on.

Employing color detection with microfluidics has proven to be a potential technique to detect the color of a liquid reagent. Microfluidic color detection is a highly sensitive and precise technique that offers many advantages over traditional methods of color detection. Traditional color detection methods often involve complex and time-consuming processes, such as chromatography or spectroscopy. In contrast, microfluidic color detection is fast, efficient, and requires only a small sample size. One key advantage of microfluidic color detection is its ability to perform quantitative analysis. By measuring the intensity of light passing through the fluid, one can determine the concentration of the color in the sample. This allows for accurate and precise measurements, which are essential for many applications in various fields, such as in clinical diagnosis or environmental monitoring. For example, in medicine, it can be used to analyze blood samples for the presence of disease markers, such as proteins or DNA. This can aid in the diagnosis and treatment of diseases. It can also be used to detect and quantify pollutants in water, air, and soil samples, which can help to identify and address environmental issues. For example, microfluidic color detection can be used to monitor the quality of drinking water or to detect the presence of contaminants in industrial wastewater. Microfluidic color detection is achieved through the use of optical sensors (an absorption-based optical sensor has been studied in this dissertation) that can detect changes in the intensity and wavelength of light as it passes through the fluid in the device. The sensors can then be used to measure the amount of color present in the fluid, which can provide valuable information about the chemical composition of the sample. Employing colorimetry to perform tests also reduces the assay time without compromising the sample volume and sensitivity. Microfluidic systems are not widespread at present; nevertheless, they are potent to become prevalent in the future and could completely revolutionize the diagnostics industry.

Most of the available color detection technologies use either a camera-based application , expensive spectrophotometric methods or are capillary-based (like chromatography)[34]. In this research, we developed an absorbance-based electronic color detection module/sensor that could be employed in microfluidic color detection using micropumps to detect the color of a liquid reagent. We also propose a detection system involving micropumps and the color sensor to perform effective color detection.

1.1 Scope of the Thesis

This thesis comprises two major works. First, a simple, low-cost color detection system for determining the color of a liquid reagent has been presented. The color sensor system is based on a light-emitting diode (LED) and a light-dependent resistor (LDR) pair to obtain information about the color of a liquid reagent. This system has been compared with a camera-based system for color detection. The LED-LDR system provides information about the color of an object by obtaining relative intensities of red, green, and blue (RGB) light reflected by the object in a sequential process. Thus, the intensity of each color component was determined relative to a two-point calibration using white and black colors. The efficacy of the system was tested by obtaining color information for different concentrations of potassium permanganate solution and by determining the endpoint of a titration experiment.

Second, we fabricated and characterized a planar, flexible, transparent microfluidic pump using polydimethylsiloxane (PDMS) as the material. The pump incorporates a nozzle-diffuser design and was fabricated as a two-layer structure: the bottom layer with the molded channels and a chamber for fluid to flow, which is encapsulated by a planar top layer. The micropump was characterized by counting the number of compression cycles required for a known volume of fluid, here water, to flow from the inlet to the outlet. The thesis also proposes a novel and cost-effective system that combines microfluidic pumps with the color sensor for detecting the color of a liquid reagent. Although the individual components required for the system have been designed and characterized, the final assembly of the system is not within the scope of this thesis. Additionally, the thesis discusses the development of a microfluidic pump that utilizes a dielectric elastomer actuator (DEA) and a tesla valve for fluidic channels to automate fluid flow. The complete fabrication process of the DEA and the pump assembly is described.

1.2 Contributions of the Thesis

- A cost-effective electronic system that can be employed in industrial settings to completely automate color detection has been assembled using an RGB light emitting diode and a light dependent resistor. A novel system architecture (depicted in Figure 2.1) has also been introduced to perform effective real-time color detection.
- A microfluidic pump featuring a nozzle-diffuser structure has been fabricated and characterized. Such micropumps have potential applications in the biomedical industry, like diagnostics, and health monitoring.
- Furthermore, we developed a new micropump that utilizes a dielectric elastomer actuator to control fluid flow and incorporates a tesla valve structure for fluidic channels. This novel design allows for more precise fluid control. Using a tesla valve-based fluidic channel for microfluidic color detection using DEA-based has not been reported earlier, to the best of our knowledge.

1.3 Organization of the Thesis

The thesis is organized as follows:

- **Chapter 2:** In this chapter, we discuss assembling a low-cost color sensor electronically using an RGB light-emitting diode and a light-dependent resistor (LDR) to perform color detection of a liquid reagent. The study also compares this system with a camera-based system and experimentally verifies the results. The LED-LDR system proved to be more robust and accurate. Hence the electronic system was used to perform some analytical chemistry experiments, and the same has been detailed in the chapter.
- **Chapter 3:** In this chapter, we look into the advantages of using a microfluidic system for determining the color of a liquid sample. Further, the chapter also discusses the development of

a planar microfluidic pump based on a nozzle-diffuser design. The complete fabrication process using polydimethylsiloxane (PDMS) is clearly demonstrated. Lastly, a novel system architecture based on micropumps and the color sensor is also proposed. This design provides a cost-effective solution for industrial colorimetry applications without compromising on the volume of the samples. However, the complete assembly of the system and characterization is not discussed and is beyond the scope of this thesis.

- **Chapter 4:** This chapter briefly introduces dielectric elastomer actuators (DEAs) and then discusses how to incorporate these actuators to design micropumps similar to those discussed in the previous chapter. Here, the nozzle-diffuser design is replaced by a tesla valve to account for the fluidic channels.

- **Chapter 5:** In this chapter, we conclude with a summary of the results discussed in this thesis.

Chapter 2

Low-cost Color Sensor for Automating Analytical Chemistry Processes

In this chapter, we will look into the development of a cost-effective and reliable electronic system to detect the color of a liquid sample in the RGB color space. This chapter involves the design, construction, and testing of an LED-LDR color detection system and compares it with a camera-based system (ESP32-CAM with OV2640 camera). An RGB LED - LDR pair was used to illuminate the sample with red, green, and blue wavelengths using a light-emitting diode (LED) and detect the intensity of the reflected light using a light-dependent resistor (LDR). The system has been calibrated to perform two analytical chemistry experiments: detecting the unknown concentration of potassium permanganate in a solution and determining the conclusion of a titration test using a photometric indicator.

2.1 Introduction

The human eye perceives color based on the wavelengths of light reflected by an object [3]. This principle has been used in the design of all optical cameras and light sensors. Because human eyes are extremely sensitive to changes in color, several chemical and medical tests are based on the color change of a solution using a color indicator. Detecting color changes in chemical reactions can help in finding the concentration of a chemical substance, or detecting the presence of a specific pathogen [2]. Thus, automatic and low-cost detection of color can be used to automate several chemical and medical tests on a large scale [38, 39, 55]. In digital communication and storage, colors are typically represented by simply identifying the intensities of component primary colors - red, green, and blue - which are represented as an 8-bit (1 byte) digital information, their values ranging from 0 (for no presence) to 255 (for maximum presence). The 16,777,216 unique colors in this system are typically represented as a three-dimensional vector (r,g,b). The highest contribution of all the three primary colors results in white color with RGB values (255,255,255), and the least contribution results in black color with RGB values (0,0,0). Though there are other color spaces like HSV (Hue, Saturation, Value), and YUV (Lua, Chroma), to quantify color, the RGB color space is the most widely used due to its simplicity and ease of use.

Detection of color change is an important tool used in several analytical chemistry processes in various industries such as biomedical, diagnostics, agriculture, food processing, and so on. Color detection can be performed using various methods depending on the application and the resources available. Several techniques have been developed to detect color, each with its advantages and limitations. Most techniques work on the principle that a colored object can either absorb, transmit or reflect a certain wavelength when monochromatic light is incident on them. The color information is obtained based on the intensity of light that falls on the photo-detector after it is absorbed or transmitted through the sample.

Most of the available color detection technologies use techniques like expensive spectrophotometric methods[10, 31, 93], colorimetry, chromatography, camera-based application or an electronic system[34]. Using an electronic system for color detection is more robust, can remove human errors, is time efficient, and can be used to automate test environments with thousands of samples. These sensors are assembled by coupling a light emitting diode (LED) to light-sensitive components such as photodiodes [33, 96, 22], photodiode arrays [20, 93], phototransistor [7, 30, 24, 32], light dependent resistors [83, 29, 89, 88, 69] in various applications that require a color detection, for example, to obtain quantitative results regarding the chemical composition of a sample. A few other previous have reported using a light emitting diode in reverse bias as a photodetector and is reported to be more sensitive compared to LED operating as a photodiode[62, 60, 63, 61]. These sensors can be integrated into a system to automate color detection and provide accurate and consistent results [76].

The work detailed in this chapter also provides a similar alternative cost-effective alternative for color detection. We present a low-cost electronic system employing an RGB light emitting diode and a light-dependent resistor to detect the color of a liquid reagent and perform a few analytical chemistry experiments.

2.2 System Architecture

We developed two separate systems, an electronic system and a camera-based system, for automatic color detection to perform a comparative analysis.

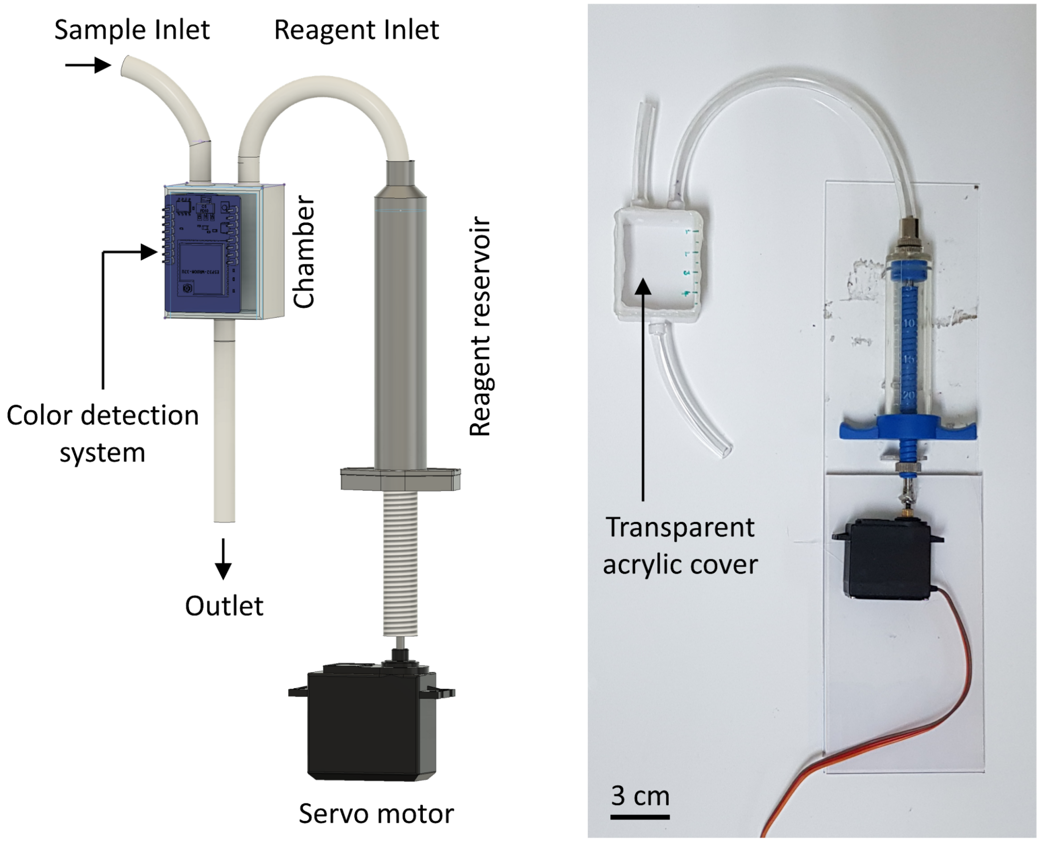

Figure 2.1: The design and the experimental setup for automatically controlled analytical chemistry processes.

The first approach involved using a camera module (ESP32-CAM, OV2640 camera) to obtain a close-range picture of the sample. The color of the sample was then estimated by finding the average of all pixel values of the captured image because the sample covered the complete field of view of the camera. The second approach involved using an LED-LDR combination to determine the intensities of the primary color constituents. Both approaches were tested using an experimental setup, shown in Figure2.1, which included a test chamber (45 mm $\times$ 35 mm $\times$ 23 mm) to accommodate the liquid sample. The chamber was fed with the sample through one inlet and the experimental reagent, if any, through another inlet using a syringe. An MG995 servo motor was used for actuating the syringe piston through a lead screw assembly. The dimensions were chosen such that the transparent face of the chamber can be fitted with the color detection module. The chamber was 3D printed using white polylactic acid (PLA) filament and sealed using a laser-cut transparent acrylic sheet. For the experiments, the sample was first poured into the chamber through one of the inlets using a fluid pump. The reagent was then injected into the chamber through another inlet with the help of a syringe. Both the inlets were electronically controlled through a central processing unit.

2.2.1 Camera-based Approach

In this approach, an ESP32-CAM camera module (from AI-Thinker), as shown in Figure 2.2a, was used to click an image of the sample through the transparent acrylic sheet. ESP32-CAM is a compact, versatile, and cost-effective solution for capturing images, and its wireless connectivity and easy programmability make it suitable for a wide range of applications like the one discussed in this study. The camera module comes with an OV2640 camera, multipurpose GPIO (general purpose input output) pins, on-chip memory , and a microSD slot. Since the ESP32-CAM does not come with a USB connector or any other in-built programmer, an FTDI programmer (Figure 2.2b) was used to serially interface the ESP32-CAM to communicate with a microcontroller (here Arduino Uno). An FTDI programmer is a UART (universal asynchronous receiver-transmitter) board that uses TTL serial communication and hence is used as a USB to TTL serial converter. For this serial communication, the Tx pin (GPIO 1) and Rx pin (GPIO 3) of the ESP32-CAM are connected to the serial pins of the FTDI for a UART communication at a default baud rate of 115000 bps. Once the interface has been successful, the FTDI can be removed. The module also had an onboard flash LED that provided the light source for the image.

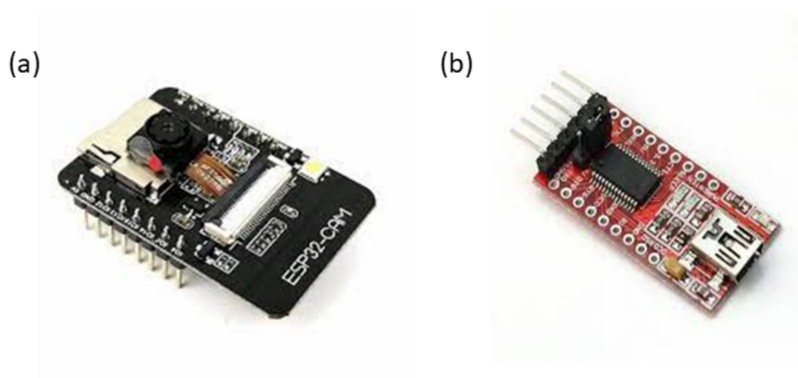

Figure 2.2: (a) ESP32-CAM (OV2640 Camera Module) (b) FTDI programmer

The pixel values of the captured image are temporarily stored as an array in the 4 MB PSRAM of the module; hence, it is essential that the dimensions of the array do not exceed the capacity of the PSRAM. With this consideration, the resolution of the image was fixed by setting the frame size to QQVGA (this can be set in the code), which corresponds to 120×160 pixels. Moreover, since writing to the PSRAM is time-consuming, the image was first captured in JPEG format and was later converted into RGB format. The values in the camera frame buffer corresponding to the captured image were converted into RGB888 format using the *fmt2rgb888* function in the ESP32 library (Since this RGB data is stored in the PSRAM, the dimension of the image was restricted to 120×160). The image can be captured by waking the ESP32 CAM from deep sleep mode by pressing the RST button, and a program that interacts with the camera module initiates the image capture process. The pixel values for each channel (red, green, and blue) can be viewed on the serial monitor of Arduino IDE. To obtain the RGB value for the sample, the average pixel values for the captured image were computed for each of the three components - red, green, and blue. Although the method discussed in this section involves directly using the values saved in the camera buffer, the captured image could also be stored on a microSD card and analyzed later as an alternative.

There are several challenges that can be encountered while clicking an image with an ESP32CAM, some of which are listed below:

- *Noise:* The images captured by the ESP32CAM can be noisy, especially in low-light conditions. This can result in poor image quality and make it difficult to identify objects or details in the image.
- *Storage limitations:* The ESP32CAM also has limited storage capacity, which can be a challenge if a large number of images need to be captured or if high-resolution images are required. The module also has a limited resolution, which may not be sufficient for some applications that require higher-quality images.
- *Connectivity issues:* The ESP32CAM relies on Wi-Fi connectivity to transfer images to other devices or the cloud. Poor connectivity or network congestion can result in slow image transfer or loss of data.

Using an expensive camera can help overcome these challenges to a great extent, but completely defies the goal of making the system cost-effective. Hence an electronic system could be a better choice.

2.2.2 LED-LDR Approach

In this approach, the color sensor was assembled using a common anode RGB LED (where red, green, and blue LEDs come as a single package, as seen in Figure 2.3b) and an LDR, as shown in Figure2.3a.

- **RGB Light Emitting Diode**: An RGB LED is available in two variants: common anode and common cathode. In the case of a common anode LED, the anode connects to a positive voltage (5V), while each of the LED pins (cathodes) to the digital output pin of a microcontroller via a resistor (here 220Ω). On the other hand, a common cathode LED has its cathode connected to the ground, and each of the LED pins is connected to the output. In the former, driving the LED pin to HIGH turns the LED on, thus sinking current, whereas in the latter, driving the pin to LOW turns it on, thus sourcing current. Even though the Arduino has the capability to sink and source the same amount of current, the sensor constructed in this study utilized a common anode RGB LED.

- **Light Dependent Resistor**: A light dependent resistor, as the name suggests, is a resistor whose resistance varies according to the intensity of light (and works on the principle of photoconductivity). The varying resistance of the LDR was measured using a potential divider circuit with a 10 kΩ resistance in series with the LDR. This value of the series resistance was chosen because the LDR resistance varies from $\sim$1kΩ to 10 MΩ for light and dark conditions, respectively (these values were obtained experimentally). The output was measured using the analog input of the microcontroller.

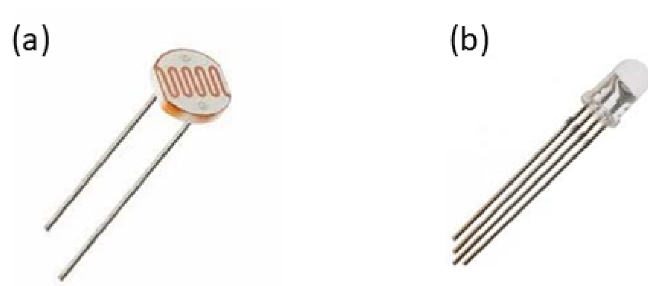

Figure 2.3: (a) Light dependent resistor, LDR (b) RGB Light emitting diode, LED

The RGB LED was programmed to switch on as red, green, and blue sequentially, and the resistance of the LDR was recorded, which corresponds to the intensity of the particular color component in the sample. While each color is emitted, the resistance of the LDR was noted using the microcontroller's analog input pin. The resistance of the LDR will vary based on the intensity of light it receives, which in turn depends on the color of the LED being emitted. The analog output from the LDR was converted into

10-bit digital information with a 3.3 V reference voltage. To compensate for experimental variations, we calibrated the LED-LDR setup using two extreme values from the RGB color space - white and black. These readings were used as the reference values for subsequent measurements (for different colors), i.e., the analog pin readings obtained when the LED emitted black and white colors were mapped to 255 and 0, respectively. Based on the reference values, the intensity of each color component was calculated relative to the calibration points, and the readings obtained for other colors were mapped to their corresponding intensity values.

Using an electronic system for color detection is more robust ad efficient; however, it has its disadvantages and challenges. Some challenges we faced when using an LED-LDR color sensor for color detection include the following:

- *Light interface:* The accuracy of the color detection can be affected by the presence of ambient light. The LED-LDR sensor may not be able to distinguish between the LED light and ambient light, leading to inaccurate color detection. Since the LDR is susceptible to external light; hence, the environment in which measurements are taken should be covered with an opaque enclosure.
- *Angle of incidence:* The angle at which the LED light hits the object being detected can affect the accuracy of the color detection. If the angle of incidence is too acute or too oblique, the color detection may be inaccurate. The LED-LDR color sensor must be positioned correctly to ensure accurate readings.
- *Limited color range:* LED-LDR color sensors can only detect a limited range of colors, which may not cover all colors in the visible spectrum. This can make it difficult to distinguish between similar shades of color.

To overcome these challenges, it is important to calibrate the sensor regularly and ensure that the sensor is positioned correctly. It is crucial to have an algorithm in place to analyze and interpret the readings from the sensor accurately. Additionally, multiple light dependent resistors could be placed around the RGB LED to analyze the data for more accuracy.

2.3 Experimental Verification

The system was tested by exposing it to various greyscale shades. These shades have the same value for the red, green, and blue components, ranging from 0 for black to 255 for white. The performances of the camera-based system and LED-LDR system are shown in Figure 2.4.

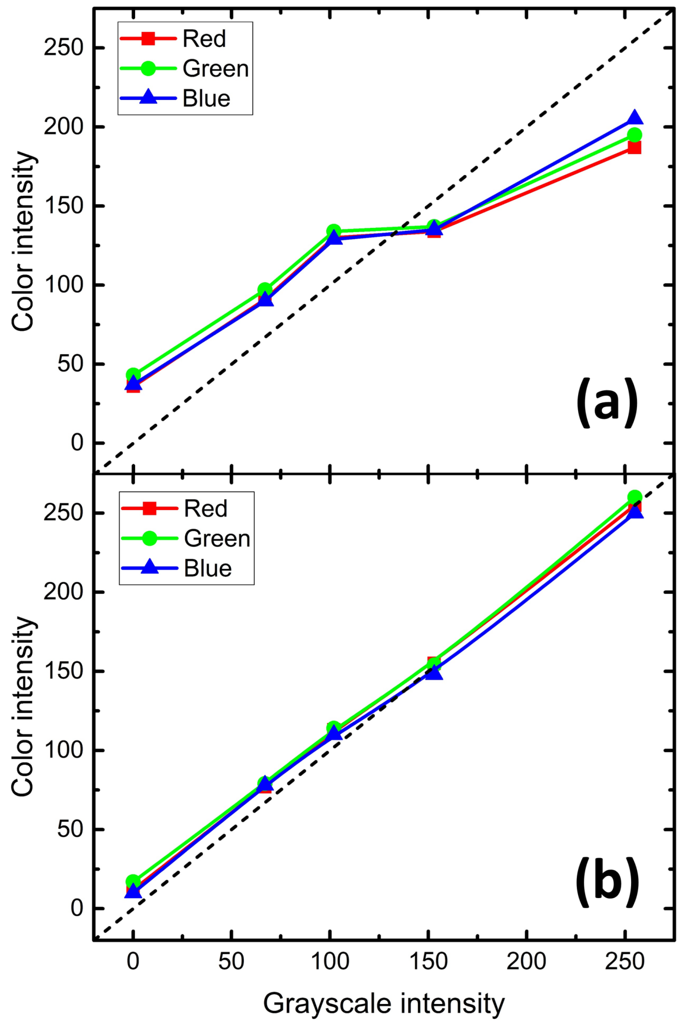

Figure 2.4: Experimental verification of the system based on the (a) Camera-based approach and (b) LED-LDR approach, shows the superiority of the LED-LDR approach.

The actual value of RGB (single value for a grey shade) is plotted on the x-axis, while the RGB output, for each primary component, is plotted on the y-axis. It can be clearly seen that the LED-LDR system performs better than the camera-based module. This can be explained by the fact that the camera-based system averages 19,200 (160×120) pixel values to obtain the intensity of each component, which can introduce errors if the image is not completely consistent. On the other hand, the LED-LDR system is based on a single sensor (LDR) that can provide robust and repeatable results, once calibrated for a specific environment. For the LED-LDR system, it was found that the maximum error among the values corresponding to all three channels was less than 8%.

2.4 Results and Discussion

Because the LED-LDR system performed much better in the experimental verification, we used this system to perform some analytical chemistry experiments. We used the color sensor to determine the concentration of a colored solution and also to indicate the endpoint of a titration experiment.

2.4.1 Concentration of a Colored Solution

For the determination of the concentration of a colored solution (colorimetry), we created aqueous solutions of potassium permanganate ($KMnO_4$) of various concentrations ranging from 0.1 mM to 0.1 M. These were made by first forming a 0.1 M concentration solution by dissolving 1.58 g $KMnO_4$ in 100 ml water, followed by appropriately diluting this solution for the desired concentration. The solutions exhibited varying shades of the characteristic purple color of $KMnO_4$. These solutions were filled in the chamber, and the RGB readings were obtained from the LED-LDR system.

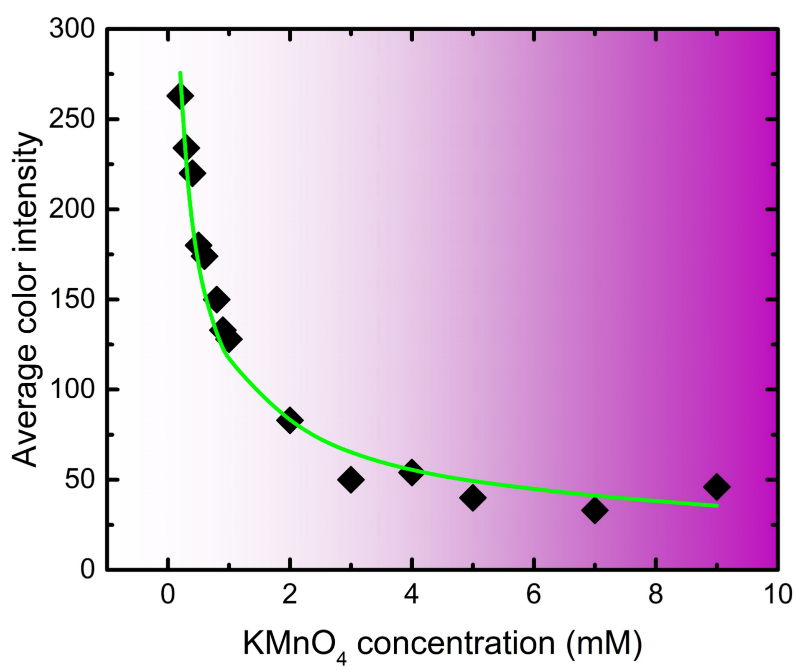

Figure 2.5: Change in measured average color intensity with $KMnO_4$ concentration. The black dots represent experimental values, the green line is the best-fit exponential function.

Because we were determining the intensity of a single shade (purple), the average of these values provides an indication of the color intensity as shown in Figure2.5. We fitted an exponential function to the experimental results so that the system can be calibrated to determine unknown concentrations of $KMnO_4$ from RGB values. It was observed that the average RGB value varies with the concentration of $KMnO_4$ according to the following equation:

$$Y = 2.82\, C^{-0.538} \tag{2.1}$$

where Y is the average color intensity and C is the concentration of the solution.

2.4.2 End Point of Titration

Titration is a commonly used technique in analytical chemistry processes [42, 15]. In this experiment, titration was performed using aqueous solutions of hydrochloric acid (HCl) and sodium

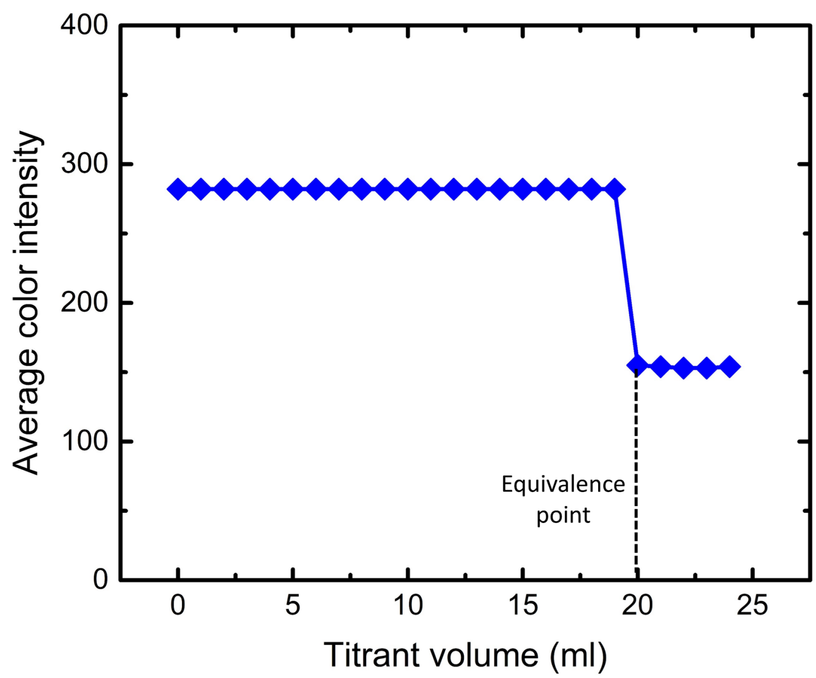

Figure 2.6: The sudden change in measured average color intensity provides an indication of the occurrence of the equivalence point of the titration.

hydroxide (NaOH), of the same molarity, with phenolphthalein as the color indicator. The indicator is colorless for acidic solutions and turns pink in basic solutions. The HCl solution was used as the analyte, and the NaOH solution, as the titrant. We introduced 20 ml HCl solution in the chamber, and the corresponding average of RGB values was noted. The titrant was then added in steps of 1 ml and the average RGB values were noted at each step. After adding 20 ml of NaOH, it was observed that the solution in the chamber turned pink, indicating that the equivalence point had been reached. The sudden change in color, as seen in Figure 2.6, is an important indication that such an experiment can be controlled algorithmically, i.e., upon detecting the change in color, the addition of titrant can be stopped.

Chapter 3

Fabrication and Characterization of a Flexible Transparent Nozzle/Diffuser Micropump

In this chapter, we will look into the details that went into the development of a flexible, transparent microfluidic system. The chapter first introduces the reader to microfluidic systems, micropumps in specific, and their applications in various domains. Further, the complete fabrication process using Polydimethylsiloxane (PDMS) and characterize the micropump. Finally, we propose a microfluidic color detection system that uses the micropumps designed in this study and the color sensor discussed in the previous chapter for effective color detection.

3.1 Introduction

Since their inception, Micro Electromechanical (MEMS) systems have had a tremendous impact on numerous fields like biochemical analysis, diagnostics, microfluidics and others [64, 80, 46].Fluidic systems are among the first MEMS-based devices that were miniaturized to a microscale. The properties inherent in fluids at the macroscopic scale, tend to show large deviations when taken in minuscule quantities or when allowed to flow through micro-scale channels. For example, when gas inclusion in liquids is present, volumetric forces such as weight or inertia frequently become irrelevant, but surface forces dominate fluidical behavior. These unique features are the key to new scientific experiments and innovations in the field of microfluidics.

Pumps are a crucial component of a microfluidic system. With emerging biomedical technology, using pumps to handle extremely small fluid amounts has become important [59]. Micropumps can be readily used in existing systems and are capable of transporting minute quantities of chemicals in a precise and safe manner which is a critical component when it comes to microfluidic systems [98]. Recent advancements in the miniaturization of electronic devices and the introduction of next-generation wearable electronics have paved the way for the development of miniature laboratories capable of instantly analyzing biofluids. This breakthrough technology, known as lab-on-a-chip devices, employs microfluidics to execute a wide range of functions, including cell analysis, molecule detection, and biochemical reaction monitoring [50, 49, 1, 47, 48, 51]. Microfluidic devices integrated with pumps are used in lab-on-a-chip devices for biomedical applications to transport small volumes of reagents and micro-total-analysis systems [56, 14]. One such scenario where such systems could be used is in implantable microsystems to transport a precise quantity of drugs/medicines inside the human body and to monitor a few biological parameters by using them in conjunction with sensors. They can also be used to perform a few chemicals, biomedical assays, and other colorimetric analyses [12, 57, 43]. Thus, the quantities of samples and reagents required to perform tests like immunoassay-based blood tests can be reduced drastically with very little manual intervention.

There are multiple kinds of micropumps, like mechanical, piezoelectric, electrostatic, pneumatic, and electromagnetic, that have been studied in the literature before. Mechanical pumps are made using a micromachining rotor-based transportation system to ensure the flow of liquids ,i.e., they use moving parts, such as diaphragms or pistons, to create pressure and move fluids. [74]. These are not restricted by the type of liquid but are often very difficult to fabricate. On the other hand, non-mechanical pumps often offer simple solutions but turn out to be restrictive due to their dependence on the characteristics of the fluid being transported [72]. Piezoelectric micropumps use piezoelectric materials that change shape when an electric field is applied, generating pressure waves that move fluid [90, 82, 6]; electrostatic micropumps use the attraction and repulsion of electric charges to move fluids [4, 66, 9]; pneumatic micropumps use compressed gas or air to move fluids [53, 99]; electromagnetic micropumps use the magnetic field generated by a coil to displace the fluid [97, 70, 5].

The nozzle/diffuser micropump is one of the most straightforward designs of a non-mechanical micropump. Due to the simplicity of their design, multiple studies have been reported in the literature characterizing their performance and employing the pumps in various applications [54, 87, 85, 58, 79]. Nozzle/diffuser pumps stand out due to their valveless design hence avoiding wear, fatigue, and clogging in the micropumps. Previous works that have studied their characterization have been either theoretical analyses or were CFD (computational fluid dynamics) simulations that perform finite element analysis to compute the desired parameters [8, 21, 44, 71]. Relatively fewer findings have been reported with experimental characterization. In particular, PDMS-based micropumps have been reported for a non-contact pumping mechanism and for manipulation of microfluidic devices using multi-layer soft lithography [58, 45, 27]. However, these reports lack information pertaining to the performance of the flexible pumps under bending. In this work, we present the fabrication and characterization of a nozzle/diffuser pump fabricated completely using PDMS. The use of PDMS provides physical flexibility, optical transparency, chemical inertness, facile fabrication, low-cost, and low gas permeability. The fluid flow per compression cycle has been studied for the pump on a flat surface and for different bending radii.

3.2 Pump Design

Any microfluidic system requires a few decisions to be made [94]. First, a method to send in liquids or reagents into the system, and for the expulsion of fluid from the system. Second, a channel for the transportation of the liquid within the system. Third, a propulsion mechanism that will drive the liquid from the inlet to the outlet. Finally, a valve system to ensure the liquid flow is in a particular direction. Once all these details have been finalized, a fabrication process is determined to realize the design.

We chose a nozzle/diffuser structure, as shown in Figure3.1, to implement the propulsion mechanism as well as the valving system. The absence of mechanical valves ensures that the liquid inside the system does not interact with any other material apart from the one used to create the chamber and the channels. Our valveless pump design features a central chamber that is connected to both an inlet and an outlet by means of two trapezoidal flow diodes. This approach allows for fluid flow control without relying on traditional mechanical valves.

The fluid present in the pump starts to flow when the central chamber is pressurized repeatedly. The inlet behaves as a nozzle, and the outlet behaves as a diffuser when the chamber is pressed. Conversely, the outlet acts as a nozzle, and the inlet behaves as a diffuser when the chamber is released. The fluid flows out of the chamber in both directions in both cases. However, because of the trapezoidal structure of the flow diodes, the amount of liquid leaving and entering the chamber is different in both directions [36, 8]. This ensures that there is net flow in one direction (from inlet to outlet), as seen in Figure 3.2

We chose PDMS as the material to fabricate the body of the pump, including the inlet and outlet chambers and the channels for liquid transport. This provided us with an opportunity to fabricate the complete system in a single step. As shown in Figure 3.3a, the pump was fabricated in two parts. The

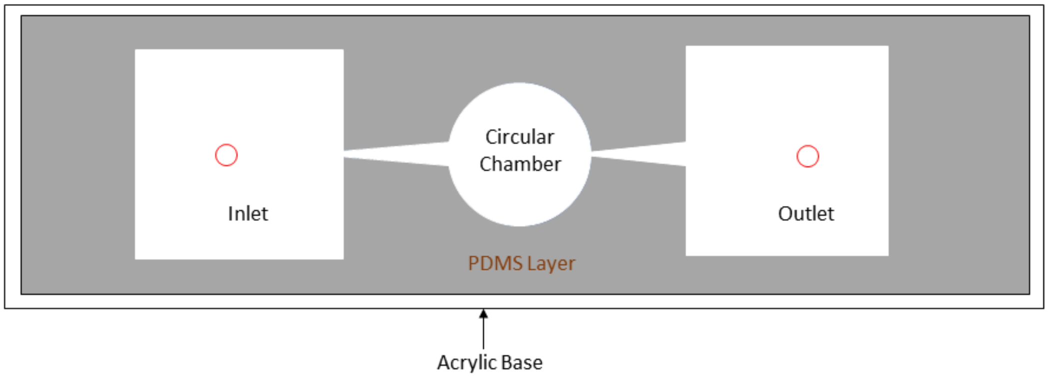

Figure 3.1: Structure of the nozzle-diffuser micropump [8]

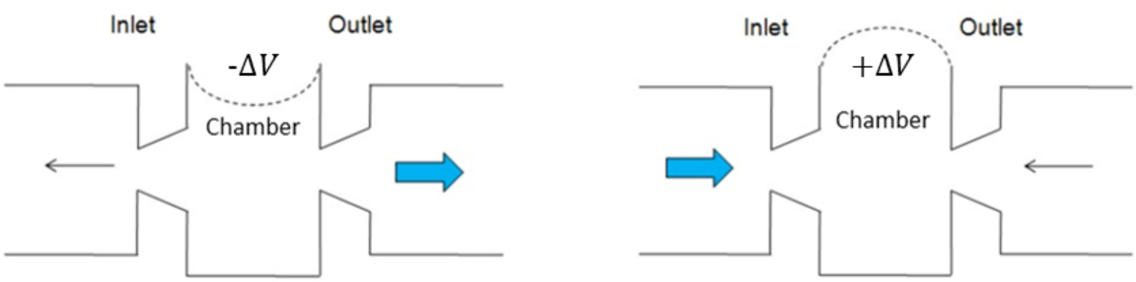

Figure 3.2: Principe of operation of nozzle-diffuser micropump.[8]

bottom part consisted of the channels, the trapezoidal flow diodes, and the chambers, whereas the top part was a thin slab of PDMS providing enclosure. Because both parts were fabricated using PDMS, the complete assembly remains flexible and transparent. The flexible nature of the top PDMS covering also ensures that there is a facile method for applying compression cycles on the chamber.

3.3 Fabrication Process

The fabrication process is schematically illustrated in Figure 3.3b. The process started with a 3D-printed mold using white polylactic acid (PLA) filament as the printing material (Ultimaker S5, print time: 1 hour). The mold was 0.7 mm thick, and the diameter of the circular chamber was 20 mm. The length of the trapezoidal structure was 150 mm, while the widths of its ends were 400 μm and 3 mm. This structure acted as the negative mold. To mold the PDMS in this structure, a parent mold was fabricated by laser cutting a transparent acrylic sheet to create a container with dimensions 15 cm $\times$ 7.5 cm $\times$ 3 mm. The negative mold was then stuck to the base of this container so that uncured PDMS can be cured around it.

The uncured PDMS mixture was prepared using the Sylgard 184 kit by mixing the base polymer and the curing agent in a ratio of 10:1 by weight. The mixture was degassed in a vacuum chamber before pouring into the container mold to cure. After the 48-hour curing process at room temperature, the patterned PDMS slab was carefully detached from the acrylic base. The top PDMS layer was then fabricated using a similar container mold without the negative mold. This top layer was attached to the mold-imprinted bottom layer using stiction between the two surfaces. Two small apertures were made on the top layer to function as inlet and outlet for fluid flow. Figure3.4a shows the images of the final fabricated pump. It can be clearly seen that the pump assembly is highly flexible and transparent. Figure3.4c shows the optical microscopy image of the trapezoidal channel connecting into the circular chamber. Such an assembly can be used for colorimetry applications by placing a light-detector pair on the top PDMS layer to detect the color of the sample in the chamber [**?**].

3.4 Results and Discussion

The final assembly of the pump was characterized by measuring the number of compression cycles required for a known volume of fluid, here water, to flow from the inlet to the outlet. The known volume of water was taken in the inlet using a micropipette. The chamber was then repeatedly pressurized, here manually, for the fluid to flow from the inlet to the outlet. Different volumes of water: 0.1 ml, 0.2 ml, 0.5 ml, and 1 ml were at the inlet, and the number of compression cycles required for the water to flow from the inlet to the outlet was recorded in each case. The experiment was repeated five times for each volume of water to obtain the average compression cycles needed. The average number of compression cycles required for these volumes was found to be 28, 49, 86, and 180, for 0.1 ml, 0.2 ml, 0.5 ml, and 1 ml water, respectively.

As shown in Figure3.5, the relationship between the average number of compression cycles with volume flow is linear, as expected. The slope of the line provides the average fluid rate expected from the pump. We report the average fluid flow per compression cycle for our design to be 5.53 μl. Such

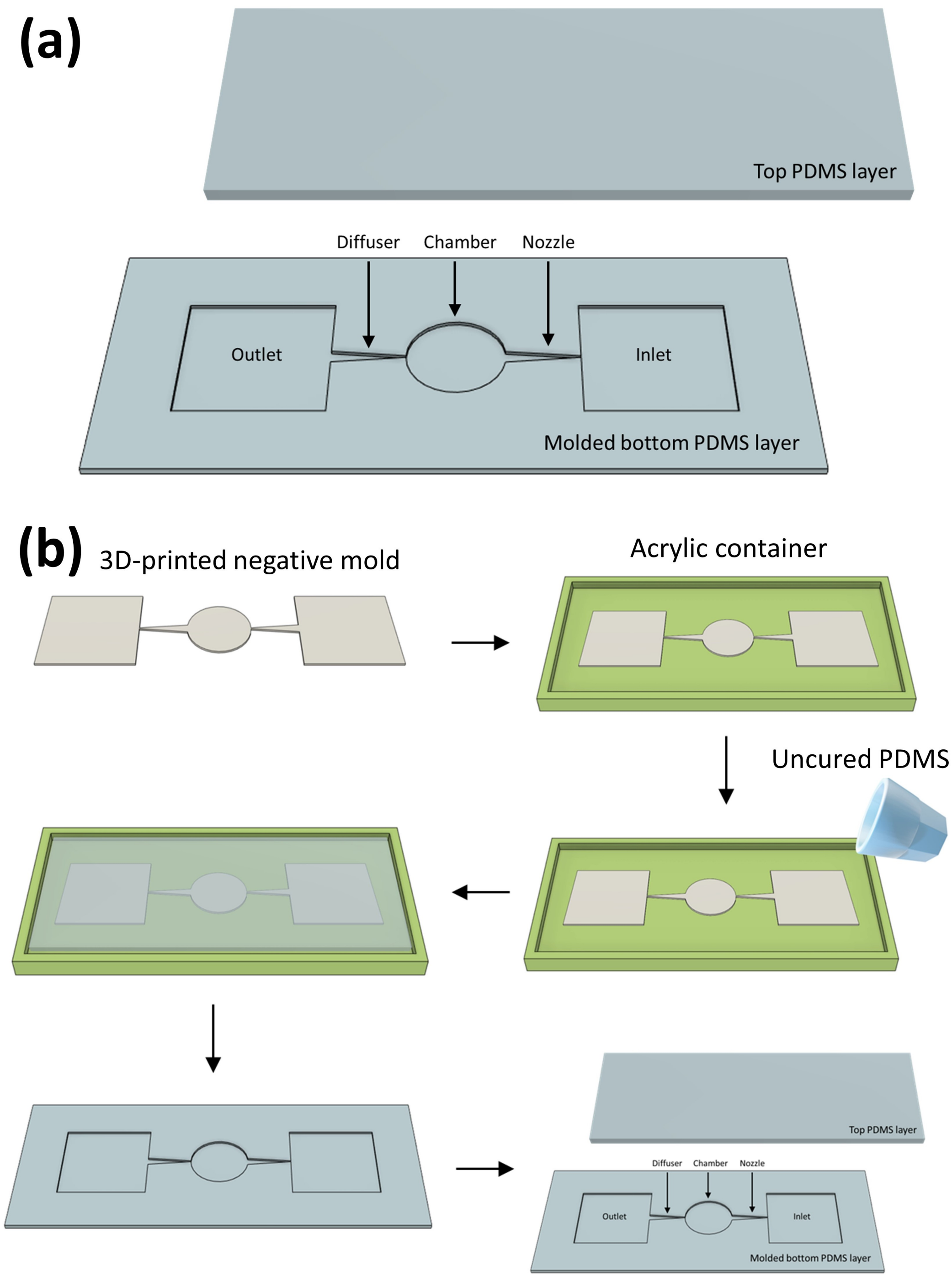

Figure 3.3: Schematic illustration of the two layers of the pump assembly.

a small flow per compression allows for precise control of the amount of fluid flow. A few previous studies have also reported that the performance of the micropump is heavily dependent on nozzle-diffuser

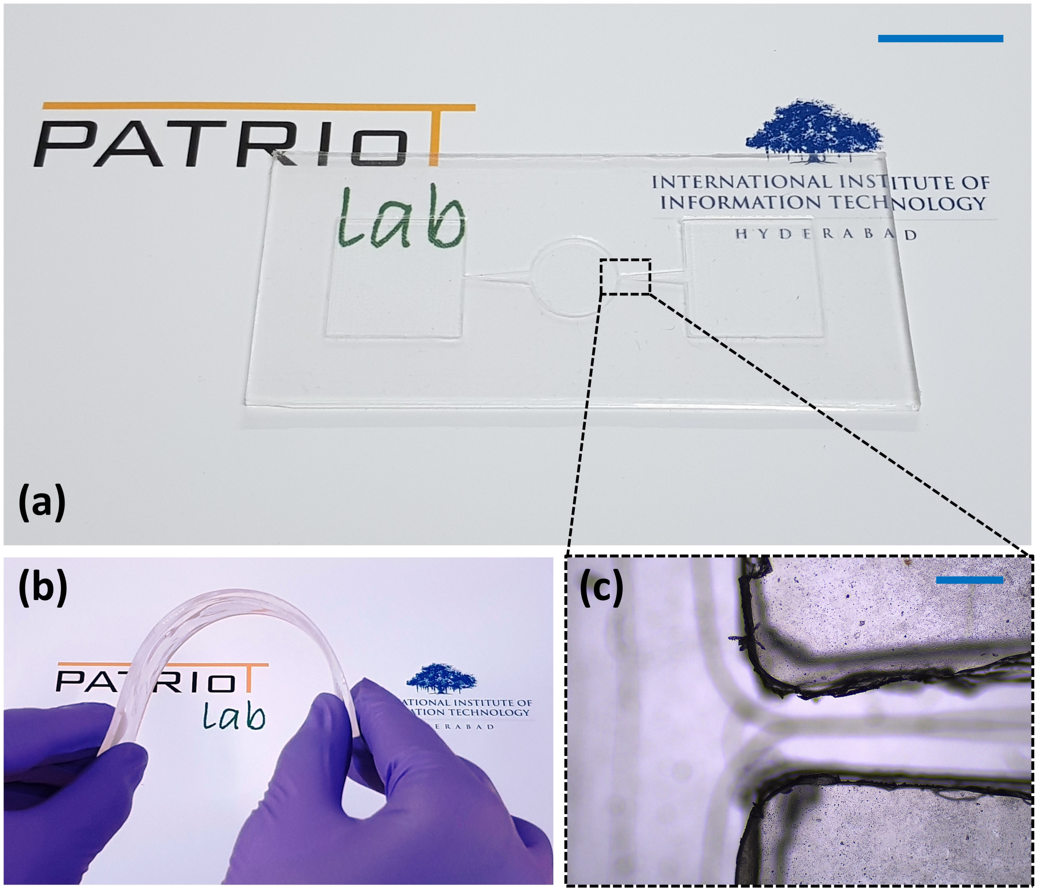

Figure 3.4: Images of the pump clearly show (a) transparency and (b) flexibility (c) Optical microscopy images show the joining of the narrow trapezoidal channel into the circular chamber. Scale bars are (a) 3 cm, (c) 500 μm.

geometry, i.e., L, W_1, W_2 [95, 54]. The efficiency of the nozzle-diffuser structure can thus be improved by analyzing the performance of the pump with different nozzle-diffuser geometries.

To verify the functioning of the pump while flexing, it was characterized while placed on surfaces of varying bending radii, which were 3D printed using white PLA filament. The pump was then placed on these surfaces to perform the experiment.A known amount of water, 0.5 ml, was taken in the inlet, and the number of compression cycles required for the sample to flow from the inlet to the outlet was noted for each case. The experiment was again repeated multiple times to report the average value for the number of compression cycles required. Figure3.6 shows the performance of the pump under different bending radii. The points represent the experimental observations, and the line represents the average

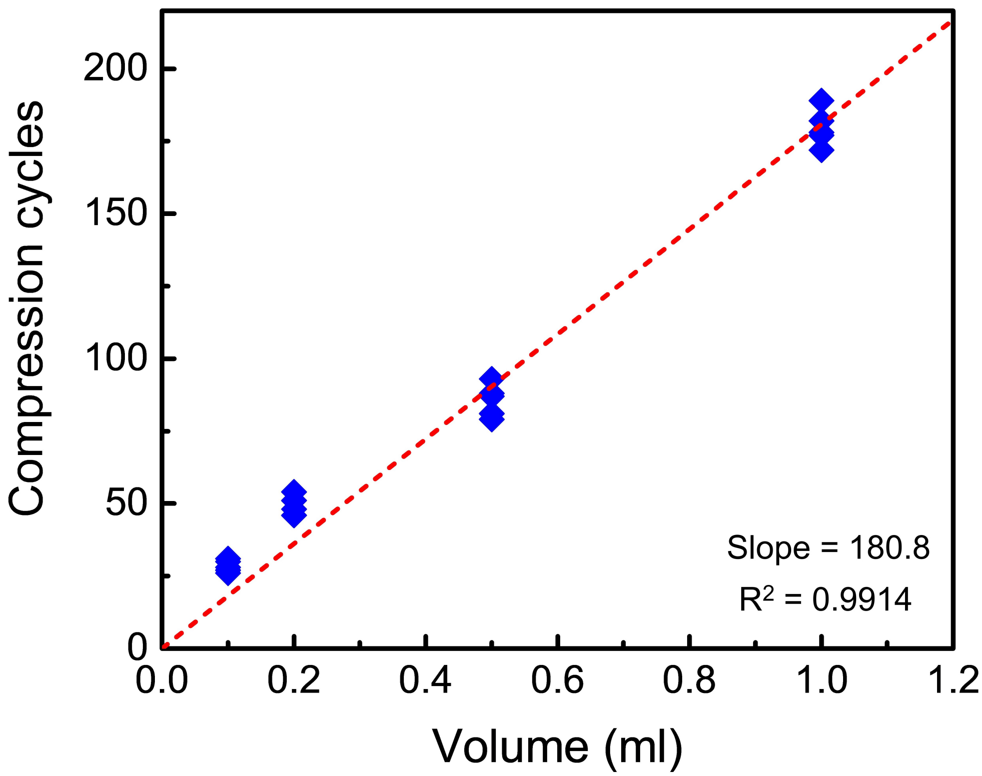

Figure 3.5: The number of compression cycles versus volume of fluid flow has a linear relationship with a slope of 180.8 ml^{-1}.

compression cycles required for 0.5 ml water at respective bending radii. We observed that the number of compression cycles required increased when the pump was subjected to higher flexing curvature. One of the reasons for this could be the reduction in effective volume compression of the chamber with strain. This change in the shape of the microchannel, when flexed, alters the flow of fluid through the device. Thus, the bending-induced deformation can cause changes in the fluid velocity within the microchannel, and these changes can impact the overall flow rate. The volume displaced in the chamber directly relates to the amount of flow obtained per cycle through the efficiency of the pump [75]:

$$V = 2 \cdot \delta v \cdot C \cdot n \tag{3.1}$$

where, V is the fluid flow, δv is the chamber volume displaced per cycle, n is the number of cycles, and C is an efficiency term related to the design of the pump. Thus, a reduction in the chamber volume displaced per cycle directly leads to a reduction in fluid flow per cycle. We report the average fluid flow

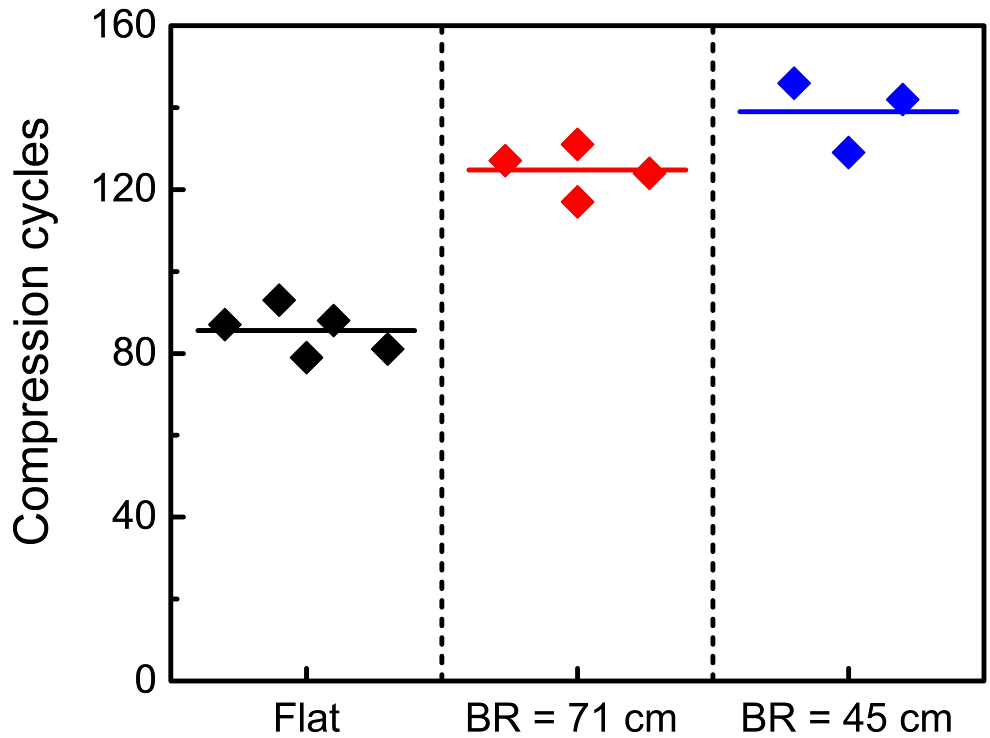

Figure 3.6: The average number of compression cycles for 0.5 ml water displacement increase with higher bending.

per compression cycle to be 4 μl and 3.6 μl for bending radii of 71 cm and 45 cm, respectively. Though it is observed that the performance of the pump is reduced when flexed, this analysis of the micropump is particularly useful in cases where bending may be used to enhance the performance of the micropump by optimizing the deformation of the membrane to achieve the desired flow rate and pressure. Furthermore, the design of the micropump can be optimized to take advantage of the deformation of the membrane when it is bent. For example, the geometry of the microchannel can be tailored to enhance the flow rate and pressure when the membrane is bent. Additionally, the material properties of the membrane can be selected to achieve the desired deformation characteristics.

Nozzle-diffuser micropumps thus have the ability to handle minuscule amounts of fluids along with the advantage of being compact. Nevertheless, we observed they also came with a few challenges. Nozzle-diffuser micropumps are susceptible to cavitation, a phenomenon in which vapor bubbles or voids form and collapse within the fluid, which can damage the pump and reduce its efficiency. The narrow channels and nozzles used in the micropump can easily become clogged with particles, debris, or air bubbles, which can impede the flow of fluid and is a major cause for degradation in the performance of the pump. This is a major issue when dealing with liquids with large viscosity. It is crucial to dislodge any blockages and clear the channels using cleaning solvents like water to improve the reliability of the pump. Moreover, the pressure generated by nozzle diffuser micropumps is typically low, which can limit their use in certain applications, such as microfluidic systems that require high pressure for efficient mixing, as described in Section 3.5. The small gaps and seals in the micropump can be prone to leaks, especially if the pump is not designed and manufactured to high tolerances. Addressing leakage in a nozzle-diffuser micropump requires careful attention to the design, manufacturing process, and maintenance of the pump.

3.5 System Architecture to perform Microfludic Color Detection

In this section, we present a system, as shown in Figure3.7, that employs these nozzle-diffuser micropumps for efficient color detection. The system consists of three micropumps, of which two are used as inlets for the sample to enter and injecting the reagent. The third one is used as an outlet to flush off the mixture after completing the experiment. The system also employs a central color detection system that uses a light-emitting diode (LED) and a light-dependent resistor (LDR) to acquire the color information (from our previous work) [68]. Thus, the use of PDMS as a structural material for the device is justified because the central chamber needs to be transparent for LED-LDR based colorimetric analysis. The sample in inlet 1 and reagent in inlet 2 flow into the central circular structure when the respective circular chambers are pressurized. After they get completely mixed in the central structure, the color detection module is used to detect the color. After completing the experiment, the mixture is flushed out through the outlet, again by repeatedly pressurizing the corresponding circular chamber. The piezoelectric disk in Figure3.7 can be replaced by a dielectric elastomer actuator for precise control.

Further, the nozzle-diffuser design could be replaced by a Tesla valve because of its advantages over the nozzle-diffuser design. Tesla valves do not have narrow nozzle-like structures and are less susceptible to clogging. They can also generate high pressures, making them suitable for applications that require high flow rates or fluid mixing, like the application discussed in this section. Adding to this, they can be easily scaled up or down to accommodate different flow rates, making them a versatile option for a wide range of applications. Thus, Tesla valves make them a promising alternative to nozzle-diffuser micropumps in microfluidic applications. However, it's important to note that Tesla valves may not be

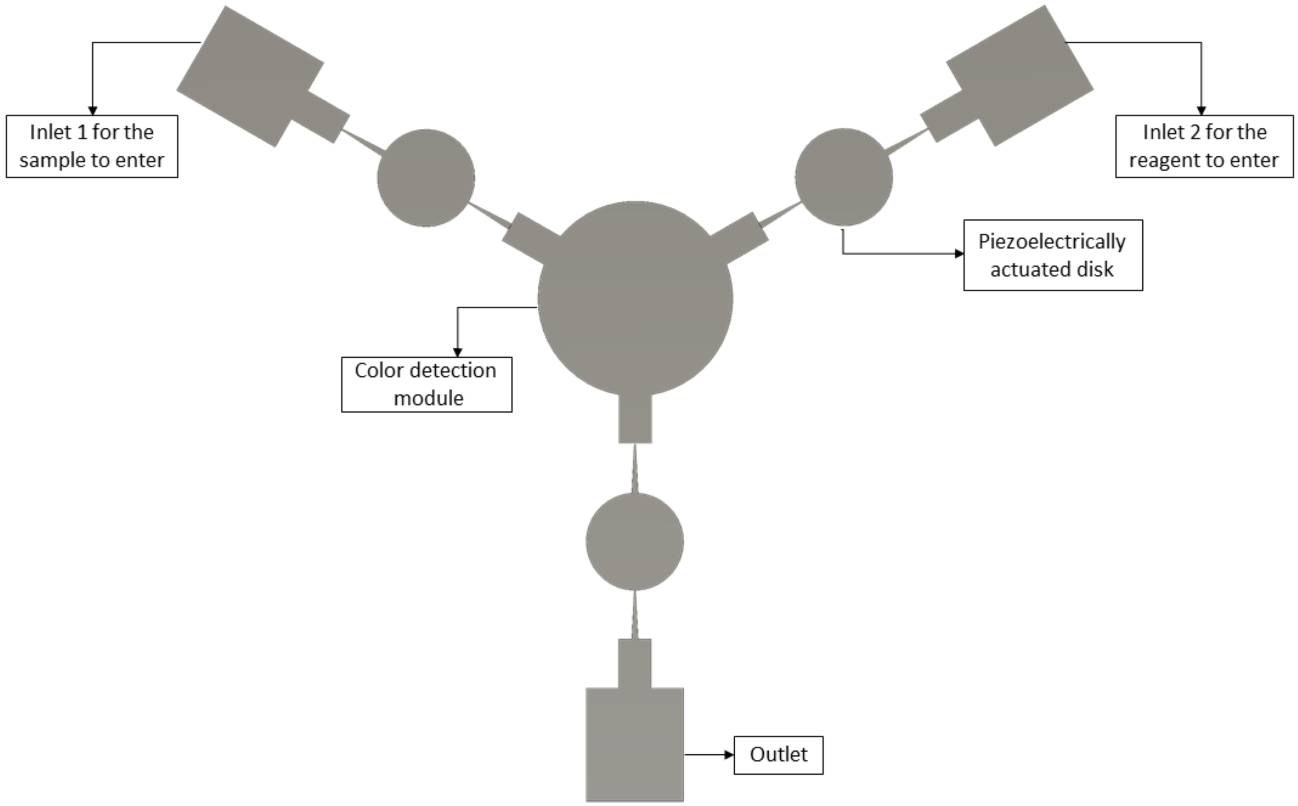

Figure 3.7: System architecture to perform color detection.

suitable for all applications, and nozzle-diffuser micropumps may still be the better choice in certain situations. The next chapter presents a detailed study on employing dielectric elastomer actuators and a Tesla valve for fluid flow.

Chapter 4

Fabrication of a Dielectric Elastomer Actuator based Micropump

In the previous chapter, we looked at designing and characterizing micropumps using nozzle-diffuser design. In this chapter, we will look at automating the mechanism for fluid flow by replacing the diaphragm with a dielectric elastomer actuator (DEA) to mimic the functionality of the diaphragm. The chapter first introduces DEAs, then details the entire fabrication and pump assembly. A similar fabrication scheme (as discussed in the previous chapter) was used to assemble the pump. Here, the nozzle-diffuser design was replaced by a tesla valve for fluidic channels.

4.1 Introduction

Dielectric Elastomer Actuators (DEAs) are a class of soft electroactive polymers that produce large mechanical strain in response to the voltage applied across its electrodes. They work on the principle of converting applied electrical energy (voltage applied) into mechanical energy because of the development of Maxwell stress in the dielectric [40, 100, 37]. The actuation strain of DEAs is typically in the range of 10-300%, which is much higher than other electroactive materials such as piezoelectric materials. Among all the thinfilm based mechanisms to impart actuation like shape memory alloys, piezoelectrics, electroactive polymer, pneumatic actuators, Metal composites, and nano-fiber-based fabrication, DEAs are the most promising due to their ability to produce large mechanical strain, low response time for a varying stimulus and high energy density. Most DEAs are based on the parallel plate capacitor configuration, wherein an elastomer layer is coated with electrodes on both sides, essentially forming a capacitor with the elastomer acting as the dielectric and the electrodes forming the parallel plates [46, 11]. Typically, the electrodes are created using mesh networks of nanotubes or nanosheets because they need

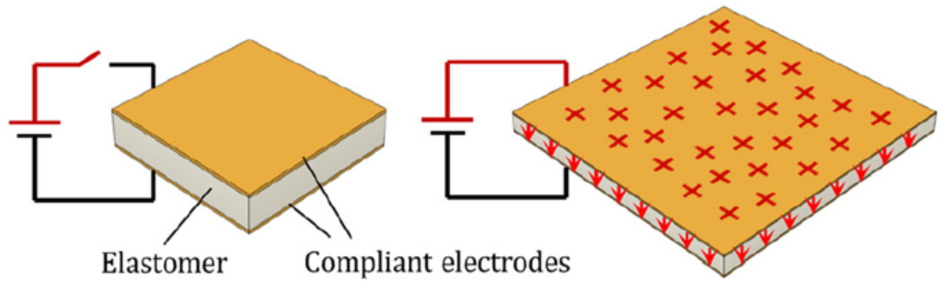

Figure 4.1: Basic principle of working of a DEA [40]

to be compliant with the large strains. When a high electric field is applied across the electrodes, the strong coloumbic forces of attraction between the charges causes the elastomer to stretch. A stack of multiple layers of elastomer and electrode, as employed in this study, can produce large displacements and actuation force for the same applied voltage.

Several DEA-based actuation applications have been reported in the literature, such as soft grippers, tactile displays, tunable lenses, and so on [25, 26, 77, 13, 18, 17]. The ability of DEAs to return to their original position once the applied voltage is removed makes it an ideal choice for a wide range of actuation applications. With some innovative designs, such as by using mechanical constraints, changing the stiffness of the material at some locations, or by using a non-uniform concentration of the electrodes applied, this in-plane deformation can be converted into an out-of-plane motion [78]. A few previous studies on out-of-the-plane actuation (or shape-morphing) introduced a passive layer along with the active elastomer-electrode stack to introduce bending due to both mechanical and electrical inhomogeneities through the thickness of the device [81, 41]. Another technique could be clamping the DEA onto a ring-like structure (for a circular DEA) to restrict the in-plane deformation. This principle was used in this design to impart the out-of-plane actuation required to mimic the function of the diaphragm (chamber) in the pump design.

4.2 Materials and fabrication

Previous studies reported dielectric elastomer actuator designs based on different elastomer materials like silicones (Sylgard 184,186, Ecoflex OO-30, OO-50) and acrylates (CN9014, CN9028), among many others[65, 52]. The precursor used to fabricate the actuators in this study comprised 99.5% CN9028, a urethane acrylate polymer, and 0.5% TPO (2,4,6-trimethylbenzoyldiphenyl phosphine oxide) as the photoinitiator. This mixture was mixed at 2000 rpm for 20 min and defoamed for 2 min at 2200 rpm using a centrifugal mixer (Thinky Mixer ARM 310). This was used as the elastomer precursor after centrifuging at 8000 rpm for 20 minutes. CN9028 offers good performance owing to its high electrical breakdown strength and low Young's modulus/low stiffness. Adding to this, CN9028 being an acrylate-based elastomer, has good adhesion with Carbon Nanotubes, unlike their silicone counterparts [**?**].

A network of percolative Single-Walled Carbon Nanotubes (SWNT CNT), carboxylic acid functionalized (P3-SWNT, Carbon Solutions, Inc.), was used as the compliant electrodes because of their ability to sustain conductivity even when subjected to large strains. The process of depositing the CNT electrodes involved sonicating and centrifuging a suspension of the SWCNT in deionized (DI) water to achieve 17% transmission with respect to DI water at 550 nm wavelength. This dispersion of CNT in DI water was then vacuum filtered using hydrophobic PTFE (polytetrafluoroethylene) membrane filters (Advantec T010A090C) with pore size 0.1 μm to form conductive CNT thin films.

4.2.1 Fabrication Process

There are several fabrication techniques reported in the literature, like spin coating, spray coating, dip coating, and inkjet printing to deposit the elastomer, and techniques like vacuum filtration and spray coating for electrode deposition. Here, spin coating was employed in the process because of its precise control over the thickness of the elastomer and ability to achieve a uniform elastomer surface profile [19]. Vacuum filtration and stamping method was used to deposit the CNT electrodes because it produces homogeneous CNT electrodes, unlike inkjet printing and spray coating where *'coffee ring'* inhomogeneities are quite common [23, 40].

The DEA was designed as a multi-layer structure by depositing alternate layers of elastomer and electrode. The entire fabrication scheme is illustrated in Figure4.2. First, the precursor was spin-coated at 2500 rpm on an acrylic substrate. It was UV cured for 180 seconds in the presence of Nitrogen gas. The thickness of each elastomer layer was $\sim 50\mu$m. Then a circular shadow mask of diameter 20 mm, laser-cut from a PET sheet using a CO_2 laser cutter, was placed on the cured elastomer layer to define the electrode geometry. The CNT electrode was then deposited by stamping a PTFE filter with CNT thin film. This filter was created by vacuum filtering 1200 μl of CNT dispersion in deionized water + 20 ml isopropyl alcohol (IPA). Finally, carefully remove the filter and the mask. These steps were repeated until the desired number of active layers, here ten, were achieved.

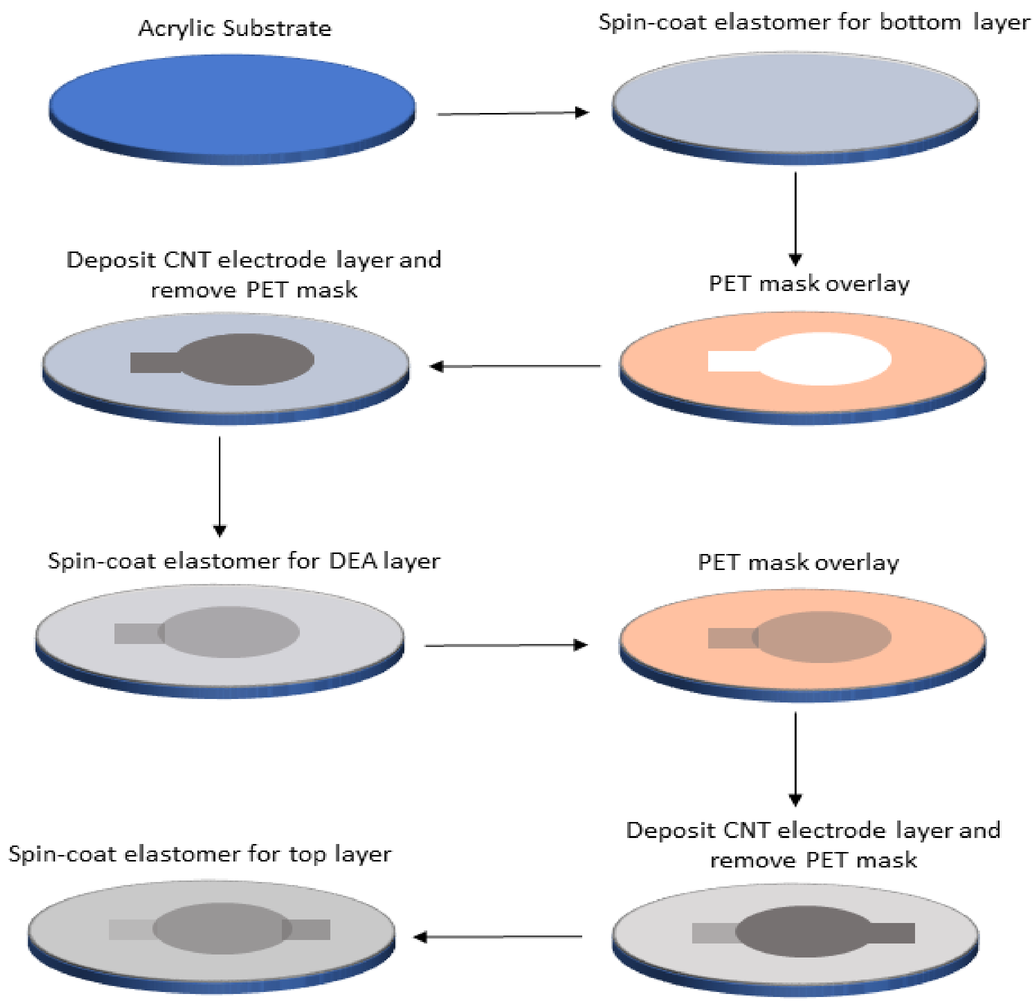

Figure 4.2: Fabrication process flow for the dielectric elastomer actuator

4.3 Results and Discussion

The fabricated actuator was tested by applying a DC voltage across the two electrodes using a high-voltage power supply after clamping it onto a ring structure that was laser-cut from acrylic using a CO_2 laser cutter. The ring structure causes the actuator to deform out-of-plane, restricting any in-plane deformation. Thus, it was observed that the actuator curls out of the plane when subjected to a large electric field. Figure4.3 shows the actuation profile of the DEA reconstructed using MATLAB simulations by processing the data obtained by scanning the surface of the DEA (when actuated) using a laser profilometer for various applied voltages. It is observed that the DEA was flat for low actuation voltages, but suddenly deforms out-of-plane that increases with voltage (0 mm for 0kV to $<$1mm at 1kV).

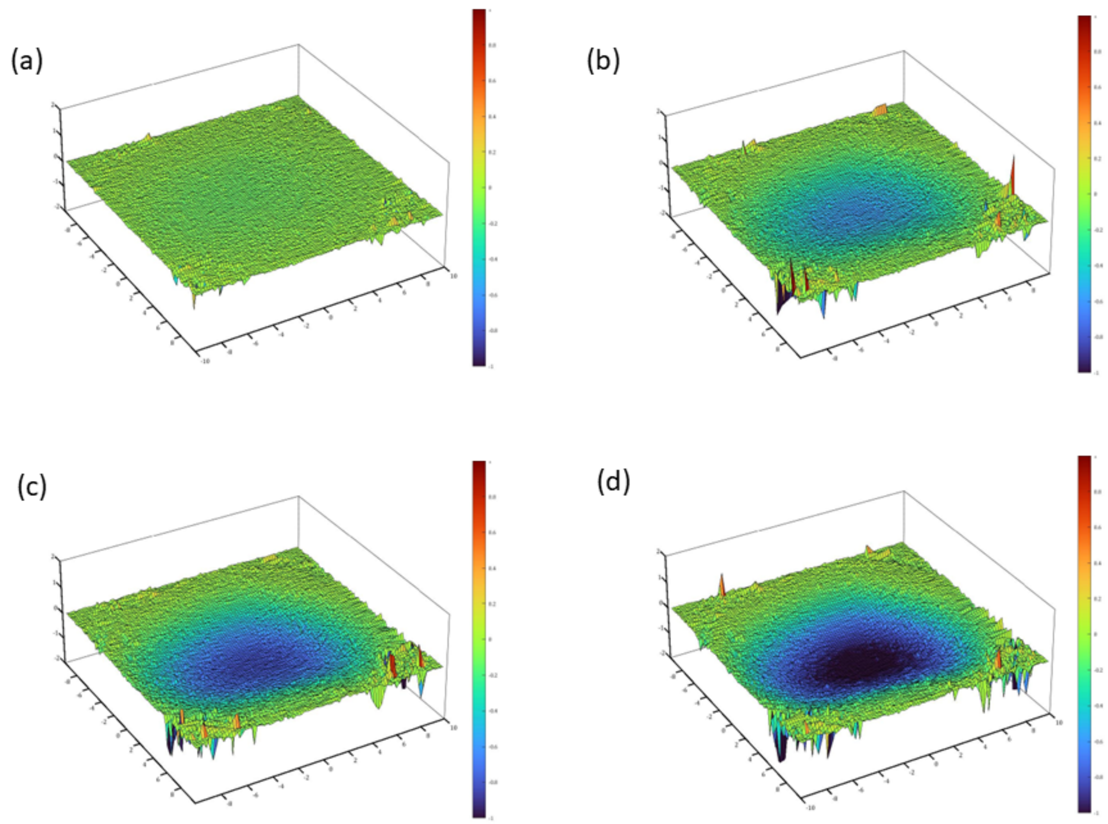

Figure 4.3: The figure shows the deformation of the actuator at various actuation voltages. (a) 0V (b) 600V (c) 800V (d)1.2kV

As with any technology, the performance of DEA is highly dependent on the fabrication process. Even small variations in the manufacturing process can result in significant differences in the mechanical and electrical properties of the device. This can cause variations in the actuation behavior, which may lead to errors or inconsistencies in the device's performance. To avoid such errors, it is important to carefully control the fabrication process and the operating conditions to achieve reliable and consistent performance from the DEA.

At sufficiently large applied voltages, the electric field produced in the elastomer exceeds its electrical breakdown strength. This causes an abrupt breakdown of the actuator. In some actuators, it was observed that there are a few current spikes at a higher actuation voltage. These are typically because of a large current passing through a localized breakdown region. The current surges in these localized breakdowns create local hotspots that change the electrode properties causing it to become non-conducting. This is called a soft breakdown and does not impact the performance of the actuator because the restriction of current causes the elastomer to *'self-heal'* by forming blisters, as shown in Figure4.4d, which can sometimes further help in improving the electrical breakdown characteristics of the complete device. These localized soft breakdowns can be caused by non-uniform polymerization/polymer cross-linking, non-uniform deposition of the metal electrode, the presence of dust particles and air bubbles are known to instigate a soft breakdown.

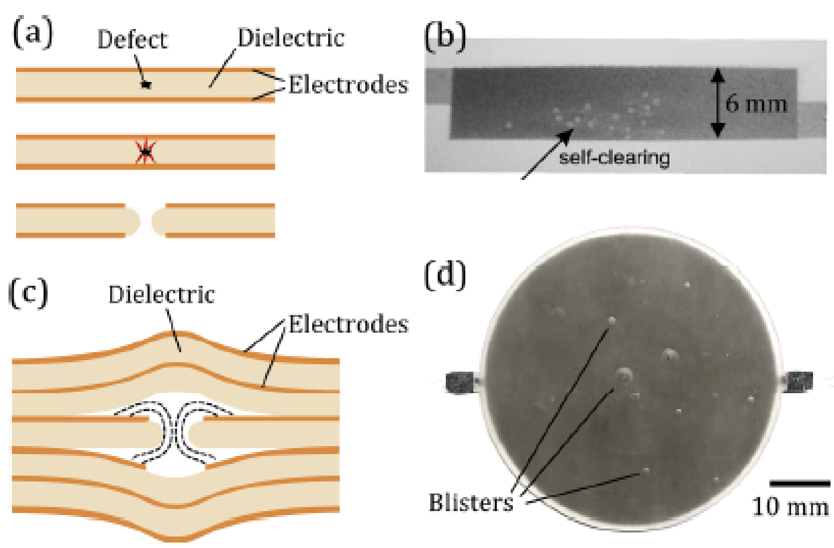

Figure 4.4: (a),(c) Self-clearing on a single-layer and multi-layer capacitor respectively (b),(d)Self-clearing in a DEA forming blisters [40, 86]

At a sufficiently large voltage, the breakdown in the elastomer layer is sufficiently large to sustain the current surge, resulting in a hard breakdown. While the hard breakdown limit is an inherent property of the elastomer material, the soft breakdown voltage of the DEA depends on multiple factors like area, elastomer thickness, and mechanical stiffness of the actuator, electrode material, fabrication process, and so on.

4.4 Micropump Design using DEA

Previous research has explored the fabrication of micropumps that employ DEAs for fluid displacement, as reported in various studies [35, 16, 28]. The design of DEA-based micropumps depends on various factors, such as the required flow rate, pressure, and the type of fluid being pumped. The key design considerations include the size and shape of the elastomer, the number and configuration of electrodes, and the fluidic channel design. The elastomer thickness is a critical factor that affects the actuation strain and the resulting flow rate. Thicker elastomers provide higher actuation force but lower actuation strain, while thinner elastomers provide higher actuation strain but lower actuation force. The number and configuration of electrodes determine the actuation direction and magnitude. A well-designed fluidic channel is necessary to minimize the flow resistance and prevent clogging.

This work introduces a novel DEA-based micropump that utilizes a tesla valve for fluidic channels. A Tesla valve is a fluidic valve with no moving parts or electrical components. It was first invented by Nikola Tesla in 1920, and its reliable operation makes it a popular choice in many industrial and scientific applications. The valve consists of a series of rectangular or circular chambers arranged in an alternating pattern, as shown in Figure 4.5. Each chamber is connected to two adjacent chambers through small channels or slots. When a fluid flows through the valve in one direction, it enters the first chamber and is forced through the channel into the second chamber. However, when the fluid tries to flow back in the opposite direction, it is blocked by eddy currents. As the fluid flows into the first chamber, it creates a vortex or eddy in the chamber, which slows down the flow of fluid and reduces its pressure. The reduced pressure causes the fluid to flow through the channel into the second chamber. However, when the fluid tries to flow back in the opposite direction, the eddy currents block the channel, preventing the fluid from passing through. This results in a one-way flow of fluid through the valve. The Tesla valve is often used in applications where a one-way flow of fluid is required, such as in pumps, compressors, and fluidic logic circuits.

The fabrication process for this pump is similar to that illustrated in Figure 3.3, with the exception of replacing the nozzle-diffuser design with a tesla valve to facilitate unidirectional fluid flow and prevent

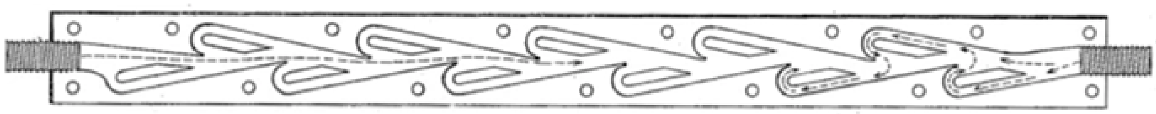

Figure 4.5: Tesla Valve [73]

backward flow, as seen in Figure 4.6. The DEA is affixed to the top PDMS slab by curing it with an elastomer (a cutout was created using a CO_2 laser cutter to accommodate the DEA). Applying a sinusoidal voltage across the DEA initiates back-and-forth actuation, creating a pressure difference, operating on the same principle as the one shown in Figure 3.2)

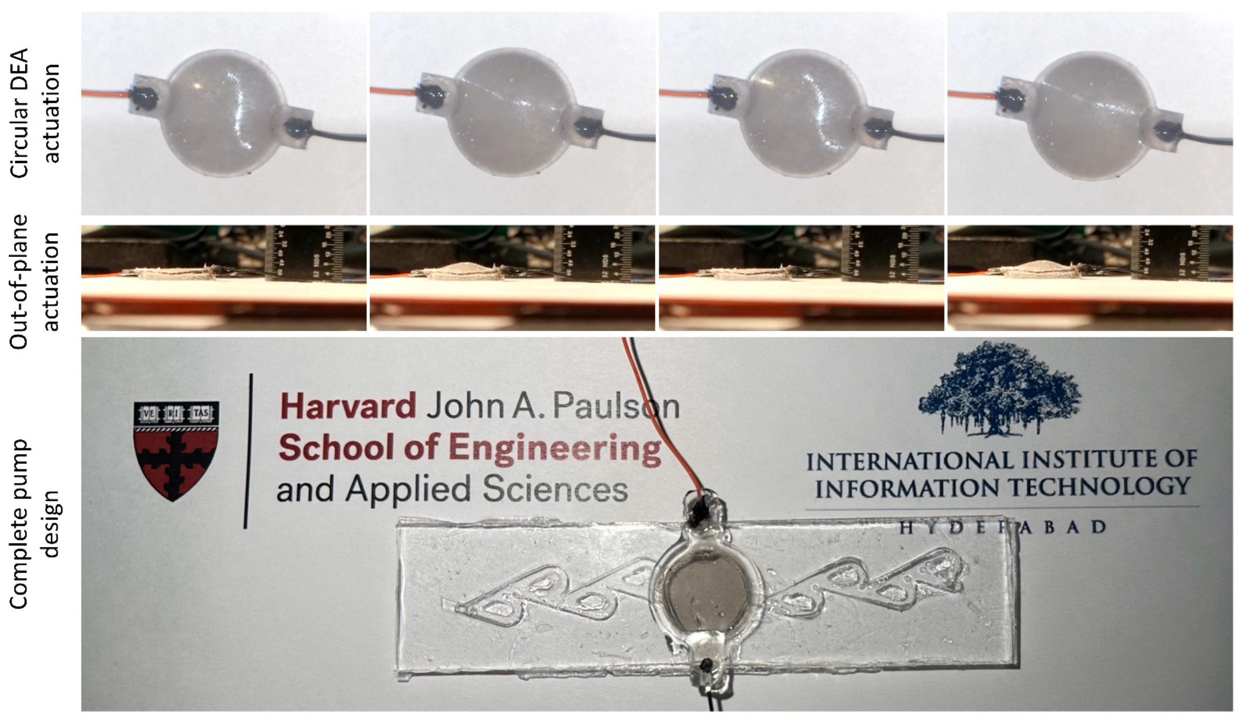

Figure 4.6: A DEA-based micropump employing a tesla valve for unidirectional fluid flow

DEA-based pumps are a promising technology, capable of achieving high flow rates, and pressure; nevertheless, they also face various challenges that limit their practical applications. One of the major challenges is the hysteresis effect, which is the difference between the actuation and relaxation curves of the elastomer. The hysteresis effect can cause a significant reduction in the pump performance, especially at high frequencies (A sinusoidal voltage needs to be applied to the DEA). Another challenge is the electrical breakdown of the elastomer, which limits the maximum operating voltage and the actuation strain. The long-term stability of DEA-based micropumps is also a concern due to the potential for material degradation and fatigue.

4.5 Future Work

More analysis is required with regards to the DEA, as there exists ample room for improvement. The fabrication technique discussed in this study can be applied to various elastomer and electrode materials, electrode shapes, and number of active layers to enhance performance. Further research will entail examining the soft and hard breakdown of the DEA, evaluating power dissipation during actuation, and studying the response of the DEA to high electric fields over extended periods. Additionally, the micropump could be analyzed to determine fluid flow versus actuation voltages at varying frequencies to achieve accurate fluid flow control. Once these are resolved, the micropump can readily be used to design the system described in Figure3.7.

Chapter 5

Conclusion

As a part of this dissertation, the design and construction of a color sensor based on an RGB LED and an LDR were discussed in detail. The results were also compared with a camera-based system to conclude that an electronic system gives more robust and accurate results. The efficacy of the system was tested by using it to determine the concentration of $KMnO_4$ solution, and by finding the endpoint in a titration experiment. As this simple low-cost system gives accurate results, it can be applied in various industrial processes that require real-time color detection and can be used to completely automate colorimetric tests like blood tests, covid tests, titrations, detecting a pollutant in water, and other industrial applications. Further, the LED-LDR pair can be fabricated on a single substrate by creating the LED/photodiodes (PD) arrays on a III-V substrate such as GaAs to obtain a compact monolithic system-on-chip (SoC) for real-time color detection.

We also presented the fabrication and characterization of a transparent, flexible PDMS-based micropump using the nozzle-diffuser design to use in conjunction with the color sensor in applications that need microfluidic color detection. The performance of the pump was characterized by measuring the number of compressions required for a known volume of sample to flow from the inlet to the outlet while placing it on a planar surface and while flexing it. The average compression cycles required for both scenarios have been reported. The complete process can be repeated for different geometries of the nozzle/diffuser. Further, the micropump can be completely miniaturized by making the inlet, outlet, and chamber by patterning a layer of SU-8 on a silicon substrate. We then propose a novel system architecture combining both LED-LDR pair and micropumps to perform color detection.

Related Publications

- **S. Malkurthi**, K. V. R. Yellakonda, A. Tiwari, and A. M. Hussain, **"Low-cost Color Sensor for Automating Analytical Chemistry Processes"**, 2021 IEEE SENSORS Conference, Sydney, Australia.
- **S. Malkurthi**, D. Niteesh, S. Bhattacharjee, and A. M. Hussain,**"Fabrication and Characterization of a Flexible Transparent Nozzle/Diffuser Pump"**, 2023 IEEE Applied Sensing Conference (APSCON), Bengaluru, India.

Other Publications

- D. Niteesh*, **S. Malkurthi***, C. Goyal, and A. M. Hussain, **"Fabrication and Characterization of a Dielectric Elastomer Actuator based Flapping Wing"**, 2023 IEEE International Conference on Flexible, Printable Sensors and Systems (FLEPS), Boston, Massachusetts, USA (submitted)
- S. Bhattacharjee, R. B. Mishra, **S. Malkurthi**, and A. M. Hussain, **"Measurement of Viscosity in Real-time using Pressure Sensors and Flow Meter"**, 2022 Students Conference on Engineering & Systems (SCES), MNNIT Allahabad, India.
- D. Devendra, **S. Malkurthi**, A. Navnit, and A. M. Hussain, **"Compact electric vehicle charging station using open charge point protocol (OCPP) for e-scooters"**, in 2021 IEEE International Conference on Sustainable Energy and Future Electric Transportation (SeFeT), Hyderabad, India.

Bibliography

[1] S. M. Ahmed, A. M. Hussain, J. P. Rojas, and M. M. Hussain. Solid state mems devices on flexible and semi-transparent silicon (100) platform. In *2014 IEEE 27th International Conference on Micro Electro Mechanical Systems (MEMS)*, pages 548–551. IEEE, 2014.

[2] S. Alamer, S. Eissa, R. Chinnappan, and M. Zourob. A rapid colorimetric immunoassay for the detection of pathogenic bacteria on poultry processing plants using cotton swabs and nanobeads. *Microchim. Acta*, 185(3):1–10, 2018.

[3] A. Amhani and Z. Iqbal. Automated color sensor system using ldr and rgb leds controlled by arduino. *ARPN J. Eng. Appl. Sci.*, 12(19), 2006.

[4] F. Amirouche, Y. Zhou, and T. Johnson. Current micropump technologies and their biomedical applications. *Microsystem technologies*, 15:647–666, 2009.

[5] I. Amrani, A. Cheriet, and M. Feliachi. Design and experimental investigation of a bi-directional valveless electromagnetic micro-pump. *Sensors and Actuators A: Physical*, 272:310–317, 2018.

[6] H. Asadi Dereshgi, H. Dal, and M. Z. Yildiz. Piezoelectric micropumps: State of the art review. *Microsystem Technologies*, pages 1–29, 2021.

[7] D. Betteridge, E. Dagless, B. Fields, and N. Graves. A highly sensitive flow-through photo transducer for unsegmented continuous-flow analysis demonstrating high-speed spectrophotometry at the parts per 10 9 level and a new method of refractometric determinations. *Analyst*, 103(1230):897–908, 1978.

[8] S. Bhattacharjee, R. B. Mishra, D. Devendra, and A. M. Hussain. Simulation and fabrication of piezoelectrically actuated nozzle/diffuser micropump. In *2019 IEEE SENSORS*, pages 1–4. IEEE, 2019.

[9] T. Bourouina, A. Bosseboeuf, and J.-P. Grandchamp. Design and simulation of an electrostatic micropump for drug-delivery applications. *Journal of Micromechanics and Microengineering*, 7(3):186, 1997.

[10] M. Bowden and D. Diamond. The determination of phosphorus in a microfluidic manifold demonstrating long-term reagent lifetime and chemical stability utilising a colorimetric method. *Sensors and Actuators B: Chemical*, 90(1-3):170–174, 2003.

[11] P. Brochu and Q. Pei. Advances in dielectric elastomers for actuators and artificial muscles. *Macromolecular rapid communications*, 31(1):10–36, 2010.

[12] M. A. Burns, B. N. Johnson, S. N. Brahmasandra, K. Handique, J. R. Webster, M. Krishnan, T. S. Sammarco, P. M. Man, D. Jones, D. Heldsinger, et al. An integrated nanoliter dna analysis device. *Science*, 282(5388):484–487, 1998.

[13] F. Carpi, C. Salaris, and D. De Rossi. Folded dielectric elastomer actuators. *Smart Mater. Struct.*, 16:S300, 2007.

[14] A. Chandrasekaran and M. Packirisamy. Integrated biophotonic utas for flow cytometry and particle detection. In *Photonics North 2009*, volume 7386, pages 25–32. SPIE, 2009.

[15] J. Chanla, M. Kanna, J. Jakmunee, and S. Somnam. Application of smartphone as a digital image colorimetric detection for batch and flow-based acid-base titration. *Chiang Mai J. Sci.*, 46:975–986, 2019.

[16] P. S. Chee, C. K. Mah, and M. S. M. Ali. Soft dielectric elastomer actuator for micropump application. In *2016 IEEE 29th International Conference on Micro Electro Mechanical Systems (MEMS)*, pages 561–564. IEEE, 2016.

[17] K. Cheng, A. Hussain, K. Burrows, and D. Clarke. Tunable blinds for windows, Feb. 18 2021. US Patent App. 16/965,531.

[18] K. Cheng, A. Hussain, and D. Clarke. Spatially and temporally tunable window devices on flexible substrates. In *Electroactive Polymer Actuators and Devices (EAPAD) XX*, volume 10594, pages 408–415, 2018.

[19] Cohen et al. Batch-sprayed and stamp-transferred electrodes: A new paradigm for scalable fabrication of multilayer dielectric elastomer actuators. *Adv. Funct. Mater.*, 32:2205394, 2022.

[20] G. E. Collins and Q. Lu. Microfabricated capillary electrophoresis sensor for uranium (vi). *Analytica chimica acta*, 436(2):181–189, 2001.

[21] P. K. Das and A. T. Hasan. Effects of flow properties on the performance of a diffuser-nozzle element of a valveless micropump. In *AIP Conf. Proc.*, volume 1754, page 040027. AIP Publishing LLC, 2016.

[22] P. K. Dasgupta, H. S. Bellamy, H. Liu, J. L. Lopez, E. L. Loree, K. Morris, K. Petersen, and K. A. Mir. Light emitting diode based flow-through optical absorption detectors. *Talanta*, 40(1):53–74, 1993.

[23] R. D. Deegan, O. Bakajin, T. F. Dupont, G. Huber, S. R. Nagel, and T. A. Witten. Capillary flow as the cause of ring stains from dried liquid drops. *Nature*, 389:827–829, 1997.

[24] S. R. B. dos Santos, M. C. U. de Araújo, and R. A. Barbosa. An automated fia system to determine alcoholic grade in beverages based on schlieren effect measurements using an led-photocolorimeter. *Analyst*, 127(2):324–327, 2002.

[25] M. Duduta, E. Hajiesmaili, H. Zhao, R. J. Wood, and D. R. Clarke. Realizing the potential of dielectric elastomer artificial muscles. *Proc. Natl. Acad. Sci. U.S.A.*, 116:2476–2481, 2019.

[26] M. Duduta, R. J. Wood, and D. R. Clarke. Multilayer dielectric elastomers for fast, programmable actuation without prestretch. *Adv. Mater.*, 28:8058–8063, 2016.

[27] M. A. Eddings and B. K. Gale. A pdms-based gas permeation pump for on-chip fluid handling in microfluidic devices. *J. Micromech. Microeng.*, 16(11):2396, 2006.

[28] S. Eom, K. Miyata, K. Asai, J.-W. Kim, and K. Yoshida. Proposal of a peristaltic micropump using dielectric elastomer actuators fabricated by mems technology. In *Electroactive Polymer Actuators and Devices (EAPAD) 2017*, volume 10163, pages 281–286. SPIE, 2017.

[29] A. Fatoni, A. N. Aziz, and M. D. Anggraeni. Low-cost and real-time color detector developments for glucose biosensor. *Sensing and Bio-Sensing Research*, 28:100325, 2020.

[30] M. A. Feres and B. F. Reis. A downsized flow set up based on multicommutation for the sequential photometric determination of iron (ii)/iron (iii) and nitrite/nitrate in surface water. *Talanta*, 68(2):422–428, 2005.

[31] L. Ferrer, G. de Armas, M. Miró, J. M. Estela, and V. Cerdà. A multisyringe flow injection method for the automated determination of sulfide in waters using a miniaturised optical fiber spectrophotometer. *Talanta*, 64(5):1119–1126, 2004.

[32] H. Flaschka, C. McKeithan, and R. Barnes. Light emitting diodes and phototransistors in photometric modules. *Analytical Letters*, 6(7):585–594, 1973.

[33] A. Fonseca and I. M. Raimundo Jr. A multichannel photometer based on an array of light emitting diodes for use in multivariate calibration. *Analytica Chimica Acta*, 522(2):223–229, 2004.

[34] A. García, M. Erenas, E. D. Marinetto, C. A. Abad, I. de Orbe-Paya, A. J. Palma, and L. F. Capitán-Vallvey. Mobile phone platform as portable chemical analyzer. *Sens. Actuators, B*, 156(1):350–359, 2011.

[35] F. A. M. Ghazali, C. K. Mah, A. AbuZaiter, P. S. Chee, and M. S. M. Ali. Soft dielectric elastomer actuator micropump. *Sensors and Actuators A: Physical*, 263:276–284, 2017.

[36] P. Gravesen, J. Branebjerg, and O. S. Jensen. Microfluidics-a review. *Journal of micromechanics and microengineering*, 3(4):168, 1993.

[37] Y. Guo, L. Liu, Y. Liu, and J. Leng. Review of dielectric elastomer actuators and their applications in soft robots. *Advanced Intelligent Systems*, 3(10):2000282, 2021.

[38] Z. Guo, Q. Ye, F. Li, and Y. Wang. Study on corona discharge spatial structure and stages division based on visible digital image colorimetry information. *IEEE Trans. Dielectr. Electr. Insul.*, (5):1448–1455, 2019.

[39] Z. Guo, Q. Ye, Y. Wang, Z. Yuan, and M. Wang. Colorimetric method for discharge status diagnostics based on optical spectroscopy and digital images. *IEEE Sens. J.*, 20(16):9427–9436, 2020.

[40] E. Hajiesmaili and D. R. Clarke. Dielectric elastomer actuators. *J. Appl. Phys.*, 129:151102, 2021.

[41] E. Hajiesmaili, E. Khare, A. Chortos, J. Lewis, and D. R. Clarke. Voltage-controlled morphing of dielectric elastomer circular sheets into conical surfaces. *Extreme Mechanics Letters*, 30:100504, 2019.

[42] G. T. Haldankar and P. Shah. A low powered auto-titrator using ph endpoint detection. In *2015 International Conference on Technologies for Sustainable Development (ICTSD)*, pages 1–3, 2015.

[43] N. A. Hamid, B. Y. Majlis, J. Yunas, A. Syafeeza, Y. C. Wong, and M. Ibrahim. A stack bonded thermo-pneumatic micro-pump utilizing polyimide based actuator membrane for biomedical applications. *Microsystem Technologies*, 23:4037–4043, 2017.

[44] X.-h. He, S.-C. Cai, Z.-D. Deng, and S. Yang. Experimental and numerical study of flow characteristics of flat-walled diffuser/nozzles for valveless piezoelectric micropumps. *Proc. Inst. Mech. Eng., Part C*, 231(12):2313–2326, 2017.

[45] S.-B. Huang and G.-B. Lee. Pneumatically driven micro-dispenser for sub-micro-liter pipetting. *J. Micromech. Microeng.*, 19(3):035027, 2009.

[46] A. M. Hussain. *Introduction to Flexible Electronics*. CRC Press, 2022.

[47] A. M. Hussain, H. M. Fahad, G. A. T. Sevilla, and M. M. Hussain. Thermal recrystallization of physical vapor deposition based germanium thin films on bulk silicon (100). *physica status solidi (RRL)–Rapid Research Letters*, 7(11):966–970, 2013.

[48] A. M. Hussain, H. M. Fahad, N. Singh, K. R. Rader, G. A. T. Sevilla, U. Schwingenschlögl, and M. M. Hussain. Exploring sisn as channel material for lstp device applications. In *71st Device Research Conference*, pages 93–94. IEEE, 2013.

[49] A. M. Hussain, F. A. Ghaffar, S. I. Park, J. A. Rogers, A. Shamim, and M. M. Hussain. Metal/polymer based stretchable antenna for constant frequency far-field communication in wearable electronics. *Advanced Functional Materials*, 25(42):6565–6575, 2015.

[50] A. M. Hussain and M. M. Hussain. Cmos-technology-enabled flexible and stretchable electronics for internet of everything applications. *Advanced Materials*, 28(22):4219–4249, 2016.

[51] A. M. Hussain, E. B. Lizardo, G. A. Torres Sevilla, J. M. Nassar, and M. M. Hussain. Ultrastretchable and flexible copper interconnect-based smart patch for adaptive thermotherapy. *Advanced healthcare materials*, 4(5):665–673, 2015.

[52] D. Ichige, K. Matsuno, K. Baba, G. Sago, H. Takeuchi, and J. Shintake. A method to fabricate monolithic dielectric elastomer actuators. In *Electroactive Polymer Actuators and Devices (EAPAD) XXII*, volume 11375, pages 295–300, 2020.

[53] O. C. Jeong and S. Konishi. Fabrication and drive test of pneumatic pdms micro pump. *Sensors and Actuators A: physical*, 135(2):849–856, 2007.

[54] X. Jiang, Z. Zhou, X. Huang, Y. Li, Y. Yang, and C. Liu. Micronozzle/diffuser flow and its application in micro valveless pumps. *Sens. Actuators, A*, 70(1-2):81–87, 1998.

[55] P. Kahar, R. Ramli, S. Etika, C. Imawan, et al. Development of color detector using colorimetry system with photodiode sensor for food dye determination application. In *J. Phys.: Conf. Ser.*, volume 1185, page 012031, 2019.

[56] P. Kawun, S. Leahy, and Y. Lai. A thin pdms nozzle/diffuser micropump for biomedical applications. *Sens. Actuators, A*, 249:149–154, 2016.

[57] J. Khandurina, T. E. McKnight, S. C. Jacobson, L. C. Waters, R. S. Foote, and J. M. Ramsey. Integrated system for rapid pcr-based dna analysis in microfluidic devices. *Anal. Chem.*, 72(13):2995–3000, 2000.

[58] J.-H. Kim, C. Kang, and Y.-S. Kim. A disposable polydimethylsiloxane-based diffuser micropump actuated by piezoelectric-disc. *Microelectron. Eng.*, 71(2):119–124, 2004.

[59] D. J. Laser and J. G. Santiago. A review of micropumps. *J. Micromech. Microeng.*, 14(6):R35, 2004.

[60] K.-T. Lau, S. Baldwin, M. O'Toole, R. Shepherd, W. J. Yerazunis, S. Izuo, S. Ueyama, and D. Diamond. A low-cost optical sensing device based on paired emitter–detector light emitting diodes. *Analytica Chimica Acta*, 557(1-2):111–116, 2006.

[61] K.-T. Lau, E. McHugh, S. Baldwin, and D. Diamond. Paired emitter-detector light emitting diodes for the measurement of lead (ii) and cadmium (ii). *Analytica Chimica Acta*, 569(1-2):221–226, 2006.

[62] K. T. Lau, R. Shepherd, D. Diamond, and D. Diamond. Solid state ph sensor based on light emitting diodes (led) as detector platform. *Sensors*, 6(8):848–859, 2006.

[63] K.-T. Lau, W. S. Yerazunis, R. L. Shepherd, and D. Diamond. Quantitative colorimetric analysis of dye mixtures using an optical photometer based on led array. *Sensors and Actuators B: Chemical*, 114(2):819–825, 2006.

[64] G. Luka, A. Ahmadi, H. Najjaran, E. Alocilja, M. DeRosa, K. Wolthers, A. Malki, H. Aziz, A. Althani, and M. Hoorfar. Microfluidics integrated biosensors: A leading technology towards lab-on-a-chip and sensing applications. *IEEE Sens. J.*, 15(12):30011–30031, 2015.

[65] G. Ma, X. Wu, L. Chen, X. Tong, and W. Zhao. Characterization and optimization of elastomeric electrodes for dielectric elastomer artificial muscles. *Materials*, 13:5542, 2020.

[66] A. Machauf, Y. Nemirovsky, and U. Dinnar. A membrane micropump electrostatically actuated across the working fluid. *Journal of Micromechanics and Microengineering*, 15(12):2309, 2005.

[67] A. Malhotra, A. S. Sandhu, and M. Singh. Development of rgb led based compact multipurpose colorimeter for hemoglobin estimation of blood. In *2019 1st International Conference on Electrical, Control and Instrumentation Engineering (ICECIE)*, pages 1–8, 2019.

[68] S. Malkurthi, K. V. Reddy Yellakonda, A. Tiwari, and A. M. Hussain. Low-cost color sensor for automating analytical chemistry processes. In *2021 IEEE Sensors*, pages 1–4, 2021.

[69] F. A. Matias, M. M. Vila, and M. Tubino. A simple device for quantitative colorimetric diffuse reflectance measurements. *Sensors and Actuators B: Chemical*, 88(1):60–66, 2003.

[70] S. Mi, H. Pu, S. Xia, and W. Sun. A minimized valveless electromagnetic micropump for microfluidic actuation on organ chips. *sensors and actuators A: Physical*, 301:111704, 2020.

[71] M. Nafea, M. S. M. Ali, T. Rehman, and K. Mehranzamir. Geometrical analysis of diffuser-nozzle elements for valveless micropumps. In *2019 IEEE International Conference on Smart Instrumentation, Measurement and Application (ICSIMA)*, pages 1–5. IEEE, 2019.

[72] N.-T. Nguyen, X. Huang, and T. K. Chuan. Mems-micropumps: a review. *J. Fluids Eng.*, 124(2):384–392, 2002.

[73] Q. M. Nguyen, J. Abouezzi, and L. Ristroph. Early turbulence and pulsatile flows enhance diodicity of tesla's macrofluidic valve. *nature communications*, 12(1):2884, 2021.

[74] J. Ni, F. Huang, B. Wang, B. Li, and Q. Lin. A planar pdms micropump using in-contact minimized-leakage check valves. *J. Micromech. Microeng.*, 20(9):095033, 2010.

[75] A. Olsson, G. Stemme, and E. Stemme. A valve-less planar fluid pump with two pump chambers. *Sens. Actuators, A*, 47(1-3):549–556, 1995.

[76] M. O'Toole and D. Diamond. Absorbance based light emitting diode optical sensors and sensing devices. *Sensors*, 8(4):2453–2479, 2008.

[77] B. J. Park et al. Monolithic focus-tunable lens technology enabled by disk-type dielectric-elastomer actuators. *Sci. Rep.*, 10, 2020.

[78] J. Pu et al. A unimorph nanocomposite dielectric elastomer for large out-of-plane actuation. *Sci. Adv.*, 8(9), 2022.

[79] K. S. Rao, K. Chandrasekharam, S. B. Sai Sri, S. Suma, M. Hamza, and K. G. Sravani. Design and performance analysis of pdms based micropump. *Transactions on Electrical and Electronic Materials*, 21:497–502, 2020.

[80] Y. Rosen and P. Gurman. Mems and microfluidics for diagnostics devices. *Curr. Pharm. Biotechnol.*, 11(4):366–375, 2010.

[81] S. Shian, K. Bertoldi, and D. R. Clarke. Dielectric elastomer based "grippers" for soft robotics. *Adv. Mater.*, 27:6814–6819, 2015.

[82] J. G. Smits. Piezoelectric micropump with three valves working peristaltically. *Sensors and Actuators A: Physical*, 21(1-3):203–206, 1990.

[83] N. Sombatsompop, N.-S. Intawong, and N.-T. Intawong. Design and construction of photo-conductive light pressure sensor for highly viscous fluids. *Sensors and Actuators A: Physical*, 102(1-2):76–82, 2002.

[84] R. J. Stanley, W. V. Stoecker, and R. H. Moss. A relative color approach to color discrimination for malignant melanoma detection in dermoscopy images. *Skin Research and Technology*, 13(1):62–72, 2007.

[85] E. Stemme and G. Stemme. A valveless diffuser/nozzle-based fluid pump. *Sensors and Actuators A: physical*, 39(2):159–167, 1993.

[86] H. Stoyanov, P. Brochu, X. Niu, C. Lai, S. Yun, and Q. Pei. Long lifetime, fault-tolerant freestanding actuators based on a silicone dielectric elastomer and self-clearing carbon nanotube compliant electrodes. *Rsc Advances*, 3(7):2272–2278, 2013.

[87] J.-H. Tsai and L. Lin. A thermal-bubble-actuated micronozzle-diffuser pump. *Journal of microelectromechanical systems*, 11(6):665–671, 2002.

[88] M. Tubino and R. L. de Souza. Determination of diclofenac in pharmaceutical preparations by diffuse reflectance photometry. *Talanta*, 68(3):776–780, 2006.

[89] M. Tubino and C. A. Queiroz. Flow injection visible diffuse reflectance quantitative analysis of nickel. *Analytica Chimica Acta*, 600(1-2):199–204, 2007.

[90] H. Van Lintel, F. Van de Pol, and S. Bouwstra. A piezoelectric micropump based on micromachining of silicon. *Sensors and actuators*, 15(2):153–167, 1988.

[91] H.-F. Wang, C. P. Xie, and K.-Y. Bian. Application of colour recognition method based on artificial neural network in the colour detection and matching system of wool fabric. *Wool Text. J.*, 1, 2006.

[92] Y. Wang. Automatic water quality arsenic element detection device based on internet of things. In *IOP Conference Series: Earth and Environmental Science*, volume 558, page 042048, 2020.

[93] B. J. White and H. J. Harmon. Optical solid-state detection of organophosphates using organophosphorus hydrolase. *Biosensors and Bioelectronics*, 20(10):1977–1983, 2005.

[94] G. M. Whitesides. The origins and the future of microfluidics. *Nature*, 442(7101):368–373, 2006.

[95] F. Xia, S. Tadigadapa, and Q. Zhang. Electroactive polymer based microfluidic pump. *Sens. Actuators, A*, 125(2):346–352, 2006.

[96] A. Yamada, M. Sakuraba, and J. Murota. Integration of si p–i–n diodes for light emitter and detector with optical waveguides. *Materials Science in Semiconductor Processing*, 8(1-3):435–438, 2005.

[97] C. Yamahata, F. Lacharme, and M. A. Gijs. Glass valveless micropump using electromagnetic actuation. *Microelectronic engineering*, 78:132–137, 2005.

[98] C. Yamahata, C. Lotto, E. Al-Assaf, and M. Gijs. A pmma valveless micropump using electromagnetic actuation. *Microfluid. Nanofluid.*, 1(3):197–207, 2005.

[99] Y.-N. Yang, S.-K. Hsiung, and G.-B. Lee. A pneumatic micropump incorporated with a normally closed valve capable of generating a high pumping rate and a high back pressure. *Microfluidics and Nanofluidics*, 6:823–833, 2009.

[100] H. Zhao, A. M. Hussain, M. Duduta, D. M. Vogt, R. J. Wood, and D. R. Clarke. Compact dielectric elastomer linear actuators. *Adv. Funct. Mater.*, 28:1804328, 2018.